Molecular and functional characterization of PCDH19 mutations in epilepsy in females with mental retardation (EFMR)

Jisoo Lim

Department of Medical Science

The Graduate School, Yonsei University

Molecular and functional characterization of PCDH19 mutations in epilepsy in females with mental retardation (EFMR)

Jisoo Lim

Department of Medical Science

The Graduate School, Yonsei University

Molecular and functional characterization of PCDH19 mutations in epilepsy in females with mental retardation (EFMR)

Directed by Professor Chul Hoon Kim

The Doctoral Dissertation
submitted to the Department of Medical Science,
the Graduate School of Yonsei University
in partial fulfillment of the requirements for the degree of
Doctor of Philosophy

Jisoo Lim

June 2019

This certifies that the Doctoral Dissertation of Jisoo Lim is approved.

Thesis Supervisor: Chul Hoon Kim

Thesis Committee Member #1: Dong Goo Kim

Thesis Committee Member #2: Heung Dong Kim

Thesis Committee Member #3: Hoon Chul Kang

Thesis Committee Member #4: Eosu Kim

The Graduate School

Yonsei University

June 2019

Acknowledgements

대학원 과정을 시작했을 때부터 끝까지 저를 지켜봐 주시고 많은 도움을 주셨던 분들께 감사 인사를 드립니다. 박사가 되는 과정 동안 필요한 지식과 많은 경험을 쌓게 해주시고, 학위 과정 내내 성심 성의껏 이끌어 주신 김철훈 교수님께 깊이 감사드립니다. 김철훈 교수님의 과학을 대하는 자세와 태도는 제가 학위가 끝난 이후에도 인생을 살아가는데 있어 큰 밑거름이 될 것입니다. 약리학 교실에서 훌륭한 업적을 이루시고 수많은 학생들을 지도하신 김동구 교수님의 퇴임을 다시 한번 축하 드리며 제가 교수님의 마지막 논문 지도 학생이 될 수 있어 매우 영광이라고 생각합니다. 임상 환자들에게 도움 주시느라 바쁘신 와중에도 소중한 시간을 내주시어 날카로운 지적과 소중한 의견을 주신 김흥동 교수님, 강훈철 교수님, 김어수 교수님께도 진심으로 감사 드립니다. 이 분들의 훌륭한 지도 덕분에 학위논문을 잘 마무리 할 수 있었습니다.

약리학교실원으로서 항상 곁에서 저에게 많은 관심 가져주시고 응원해주신 김동구 교수님, 이민구 교수님, 박경수 교수님, 김철훈 교수님, 김주영 교수님, 지헌영 교수님, 김형범 교수님께도 감사드립니다. 교수님들과 한 공간에서 연구할 수 있었던 것 자체가 저에겐 큰 배움의 기회였습니다.

학위 기간 동안 힘든 순간들이 많았지만, 지금에서 돌이켜 보면 제가 성장하고 배울 수 있었던 소중한 시간들이었습니다. 랩 생활을 시작하면서부터 정신적으로 랩 엄마처럼 저를 지지해 주시던 조아련 박사님, 실험적으로 많은 것을 가르쳐 주고 항상 칭찬과 격려를 아끼지 않았던 신소라, 윤은장, 윤종진, 김지윤, 왕혜진 선생님들께도 진심으로

감사의 인사를 전하고 싶습니다. 학위과정 동안 바로 옆에서 같이 동거동락 하며 울고 웃으며 응원해준 장유진, 김희옥, 권순성 선생님, 현종, 신원, 지인이와 함께 할 수 있어서 항상 큰 버팀목이었고 무사히 박사과정을 마무리 할 수 있었다고 고마움을 전하고 싶습니다. 연구실 식구들 한웅수 박사님, 윤송이, 김서영, 최다빈, 김소영 선생님들께도 감사의 말씀 드리며 다들 서로 응원하며 학위과정을 잘 마무리 하길 기원한다는 말을 전하고 싶습니다. 같은 실험실은 아니었지만 과정을 함께 해주었던 김유진, 유세영, 박민경, 조소연 선생님, 바쁘다는 핑계로 항상 자주 보지 못한 친구들과 소희언니, 혜인언니, 소운이 덕분에 많은 힘이 되었고 웃을 수 있었습니다.

마지막으로 위기가 올 때마다, 변함없이 격려와 지지를 아끼지 않은 부모님, 남동생과 규영이가 많이 생각납니다. 그때 마다 저의 옆을 지켜주고 보살펴 준 가족이 있었기에 여기까지 달려올 수 있었습니다. 우리가족 너무 사랑하고 앞으로 제가 받은 이 넘치는 사랑을 꾸준히 돌려줄 것을 약속하는 마음을 담아 이 논문과 사랑을 함께 전합니다.

이렇게 감사의 글을 쓰다 보니 길다면 길고 짧다면 짧은 우여곡절 많았던 5 년동안 감사할 분들이 너무나도 많은 것 같습니다. 여기에 다 쓰지 못한 다른 분들에게도 감사의 마음을 전하며, 이렇게 많은 분들의 도움을 받아 학위 과정을 끝낼 수 있었다는 사실에 새삼 마음이 뭉클해집니다. 앞으로 저도 인생을 살아가며 많은 이에게 도움이 되고 제가 받은 많은 사랑과 격려를 나눠줄 수 있는 사람이 되겠습니다.

TABLE OF CONTENTS

LIST OF FIGURES

LIST OF TABLES

ABSTRACT

Molecular and functional characterization of PCDH19 mutations in epilepsy in females with mental retardation (EFMR)

Jisoo Lim

Department of Medical Science
The Graduate School, Yonsei University

(Directed by Professor Chul Hoon Kim)

Epilepsy in females with mental retardation (EFMR) is an epileptic disease that has infantile seizure onset, often accompanying intellectual disabilities. EFMR is caused by mutations in the protocadherin19 (PCDH19) gene on X-chromosome. PCDH19 is a transmembrane adhesion molecule, dominantly expressed in the central nervous system (CNS). To date, more than 100 mutations of PCDH19 have been reported in EFMR patients and half of these mutations are missense mutations. Most of PCDH19 missense mutations are suggested to be a loss of function at the cellular levels, but neither biochemical mechanisms of pathogenic missense mutations nor its adhesive functions are still very ambiguous. EFMR is known to have extremely unusual X-linked inheritance patterns, whereby only heterozygous females are affected but not males. The pathogenesis of EFMR is supported by the theory of 'cellular interference', although it has not been experimentally established. The theory of cellular interference is that two different alleles interact to produce an

abnormal phenotype. Therefore, co-existence of two distinct populations of normal and mutated PCDH19 expressing cells could alter the proper cell-cell interactions in the brain to produce harmful effects.

Since, *PCDH19* is subjected to random X-chromosome inactivation, affected heterozygous females would have tissue mosaicism. However, the cellular mechanism related to the pathogenesis of EFMR is still unclear. Here, in part 1 of my thesis, I not only show the developmental regulation of PCDH19 expression that are critical in early brain development, but also its adhesive features. I found some of missense mutations are shown to be a gain of function through *in vitro* aggregation assay; they promote the formation of aberrant cell aggregates in the artificial mosaic environment. In part 2, I demonstrated the segregated patterns of WT and null PCDH19 cells in heterozygous female mouse brains that are associated with their higher seizure susceptibility. Taken together, these results demonstrated that the transcellular imbalance of higher (missense mutations) or lower (nonsense mutations) PCDH19 expression at the cell surface in heterozygous mutant females aberrantly interact with PCDH19 WT cells to promote abnormal cell-cell interaction in causing EFMR.

Key words: EMFR, intellectual disability, PCDH19, mosaicism, epilepsy, cellular interference, X-inactivation

Molecular and functional characterization of PCDH19 mutations in epilepsy in females with mental retardation (EFMR)

Jisoo Lim

Department of Medical Science
The Graduate School, Yonsei University

(Directed by Professor Chul Hoon Kim)

I. INTRODUCTION

A complex cell-cell interaction is essential in the development of the vertebrate nervous system. The establishment of functional neuronal architecture and connectivity are highly dependent on the interaction of the adhesion molecules that coordinate many biological processes, including cell proliferation, migration, synaptogenesis and formation of neural circuits.[1-3] Although the exact cellular mechanisms underlying these complex developmental processes are still unclear, the cadherin (calcium-dependent cell adhesion) molecule have been shown to have important roles in early embryonic development.[4-6] Protocadherins (PCDHs) are the largest group within cadherin superfamily and composed of two subgroups; clustered (C) and non-clustered (NC) PCDHs.[7] Mutations of NC PCDH family have been associated with many neurological diseases such as mental retardation, autism, schizophrenia, and epilepsy.[8,9] PCDH19 belongs to the non-clustered delta(δ)2-

protocadherin subclass of the cadherin superfamily which is located on the X-chromosome (Xp22.1) and expressed in the developing brain.[7,8,10,11] Both missense and nonsense mutations in *PCDH19*, have been reported to cause epilepsy and mental retardation limited to females (EFMR).[8] The δ2-protocaherins are known to regulate the synapse dynamics. A complex of N-cadherin and arcadlin (activity-regulated cadherin-like protein, rat homolog of PCDH8) can regulate the stability of synapses that enhances spine dynamics.[12] Also PCDH10 acting with PSD-95 (postsynaptic scaffolding protein-95) is involved in synaptic elimination.[13] PCDH17 is expressed at presynaptic regions of the excitatory and inhibitory synapses of the basal ganglia nuclei and *Pcdh17* KO mice studies have revealed that PCDH17 regulates presynaptic vesicle assembly and synaptic transmission efficacy in corticobasal ganglia.[14] However, the synaptic function of PCDH19 is still unclear. Previously, PCDH19 was suggested to be a homophilic adhesion molecular *in vitro.*[15] However, adhesive structures of PCDH19 were only recently determined to be somewhat similar to the clustered PCDH group,[11] but still not much have been known about the adhesive characteristics of the PCDH19. Approximately 50% of all reported mutations related to EFMR are missense mutations and these are distributed throughout the extracellular domains of PCDH19, yet how these various of missense mutations leads to EFMR are barely known. Recently, the adhesive properties of few EFMR-causing *PCDH19* missense mutations completely abolished PCDH19-mediated cell adhesion in *in vitro* aggregation assays. In addition, PCDH19 form heterotypical *cis* interactions with NC PCDHs and these generate specific binding affinities, causing cells sorting.[11,16]

EFMR is characterized by an infantile onset epilepsy that frequently accompany intellectual disability and autism.[17,18] Unlike the typical X-linked diseases, in which

males are affected and females are unaffected carriers, it has very unique inheritance patterns affecting only heterozygous (HET) females, not males.[8,17,19] *PCDH19* undergoes random X-chromosome inactivation in females,[8,20] therefore affected females have both the wild-type (WT) or mutant *PCDH19* allele, causing cellular mosaicism in the brain.[19] This mosaicism of normal and PCDH19 mutant cells in the brain is thought to be a strong pathogenic mechanism of EFMR, altering the normal cell-cell communication through abnormal cellular interference. This is further supported by the case of male with somatic mutation in *PCDH19*, mimicking mosaicism in HET females, also displayed typical EFMR seizure symptoms.[19] Therefore, this abnormal cellular interaction between two different populations of PCDH19 expressing cells are called 'cellular interference' mechanism, but the experimental support for this model is very limited.

Pcdh19 KO mouse models showed no apparent disturbance in gross morphological brain structures and displayed no obvious seizure phenotypes.[21,22] Only one study group conducted several behaviour tests with *Pcdh19* KO mice model and reported that both *Pcdh19* hemizygous KO male and HET KO female mice were hyperactive and HET KO female mice showed decrease in fear responses. However, other behaviour tests regarding anxiety and spatial working memory in *Pcdh19* HET KO female mice were normal.[22]

Here, I sought to address some of these questions by conducting the corresponding *in vitro* and *in vivo* experiments to investigate the characteristics of PCDH19 and its mutations and the molecular mechanism behind its unique inheritance patterns of EFMR. Therefore, in part 1 of my thesis, I aimed to establish the molecular characteristics of PCDH19 and its mutations. I showed that PCDH19 is regulated by secretase-dependent cleavage process, like other cadherin superfamily proteins,

whereas some PCDH19 missense mutations like V441E and N557K increased the surface expression levels and they become resistant to secretase-dependent cleavage. Moreover, I conducted cell aggregation assay to assess the adhesion ability of PCDH19 and some of the missense-mutated PCDH19 molecules to mediate cell adhesion. I found that a group of missense mutations promotes abnormally enhanced cell aggregates only when they are mixed with PCDH19-WT expressing cells. In part 2, I showed exclusive cell segregated patterns in the *tdT-Pcdh19* recombinant HET KO female mouse brain that are possibly induced by sorting of WT and *Pcdh19* null cells. This unique sorting pattern of cells during early mouse brain development in the HET KO female phenotypically associated with higher seizure susceptibility in the pilocarpine-induced model. Together, these results allow me to have a better understanding of the function of PCDH19 in causing EFMR.

II. MATERIALS AND METHODS

1. Animals

All experiments were carried out with wild-type (WT) and PCDH19 knock-out (KO) mice. *Pcdh19* KO mouse (TF2108); B6;129SvEv-Pcdh19tm1 was purchased from Taconic Biosciences. For breeding, PCDH19 WT(XY) or KO(X'Y) males and heterozygote (XX') female mice were crossed to obtain littermates of all genotype littermates of XY, hemizygote mutant (X'Y) for male, WT (XX), HET(XX') and KO(X'X') for female mice. Offspring were genotyped by polymerase chain reaction (PCR) amplification using three primers: common primer for PCDH19 WT and null alleles: P1, F-5′-CGA GTC CAC TAC CGA CTC TGC T-3′, for PCDH19 WT allele: P2, R-5′-AGC CCG GCT ACT CAG TTT TCC-3′, for PCDH19 null allele: P3, R-5′-CTG CAA AGG GTC GCT ACA GAC G-3′. PCR products were separated on a 2% agarose gel. PCDH19 WT and null allele products were 130 bp and 380 bp, respectively. All mice were housed in groups of 2–5 per cage with *ad libitum* access to food and water, in a humidity- and temperature-controlled, specific pathogen-free environment (12 hr light cycle; lights on at 8 am) in the Yonsei-University College of Medicine Animal Care Facility accredited by the Association for Assessment and Accreditation of Laboratory Animal Care (AAALAC). Animal cages were changed by experimenters once a week. All animal experiments were approved by the Animal Care Committee of Yonsei University College of Medicine using US National Institutes of Health Guidelines.

A. Generation of recombinant mice

Animals with B6;129-Hprt$^{tm2(CMV\text{-}tdTomato)\ Nat}$/J genetic background (Hprt-tdT mouse, JAX; stock# 021428) and B6.C-Tg(CMV-cre)1Cgn/J genetic background (CMV-cre, JAX; stock# 006054) mouse were purchased from Jackson Laboratories. Firstly, CMV-Cre mice were crossed with Hprt-tdT to remove LoxP-stop-LoxP (LSL) to generate CMV-Cre; HPRT$^{LSL\text{-}tdT}$ in order to activate tdTomato (tdT) in all cells (Figure 1, top left). Then CMV-Cre; HPRT$^{LSL\text{-}tdT}$ female mice were crossed with *Pcdh19* KO male mice (Figure 1, top right). Through a random X-chromosome dependent recombination between *Pcdh19* and tdT genes occurred to generate the two different recombinant male mice; X'$_{tdT}$Y (KO-tdT) and X$_{tdT}$Y(WT-tdT). X'$_{tdT}$Y mouse have *Pcdh19*-null and tdT genes on the same X-chromosome, and X$_{tdT}$Y mouse have *Pcdh19*-WT and tdT genes on the same X-chromosome (Figure 1, bottom). Hprt and PCDH19 were co-genotyped by PCR with 2 primers. For Hprt allele, P1, F-5′-AAG GGC GAG ATC CAC CAG -3′ and P2, R-5′-AGT CGA GGA AGC TTA AGC GTA GTC- 3′, for primers of PCDH19 allele were already described above. PCR products were separated on a 2% agarose gel, Hprt-tg product was deigned to be a 350 bp. Only recombinant males with *Pcdh19* (WT or null allele) and tdT recombinant X-chromosome are used to cross with XX' *Pcdh19* female mouse to generate recombinant female mice of all three genotypes; X$_{tdT}$X (WT), X'$_{tdT}$X (HET), X'$_{tdT}$X' (KO). In order to prevent random X-chromosome recombination from re-occurring, recombinant female mice weren't used in any of the mating process. Only the offspring from XX' and recombinant males (X'$_{tdT}$Y or X$_{tdT}$Y) mating were used in this study.

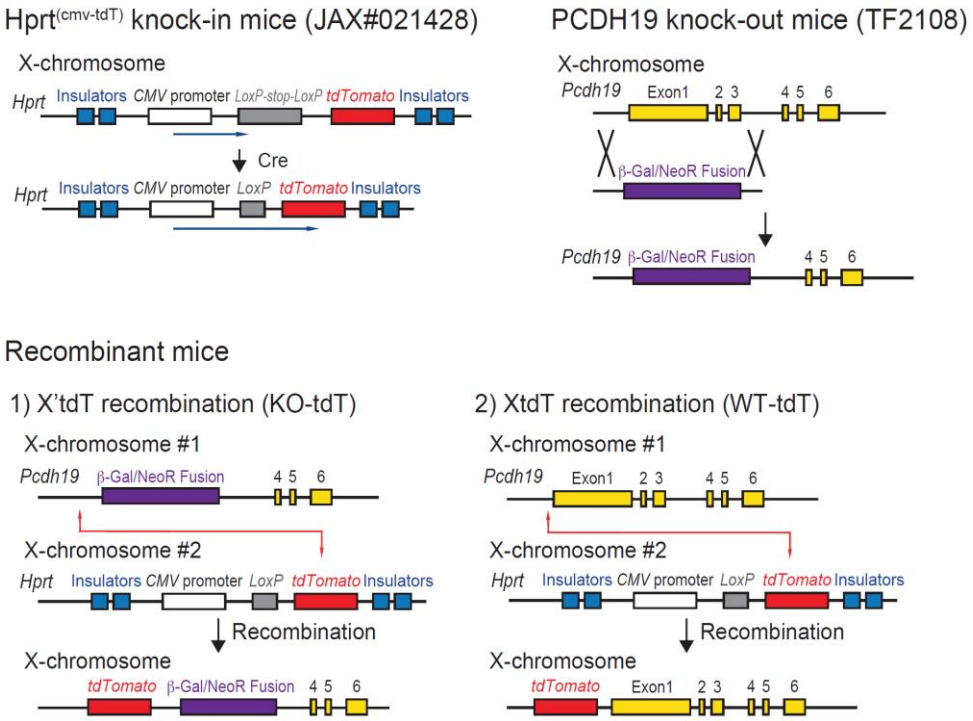

Figure 1. Generation of a *tdT-Pchd19* recombinant mouse. Strategic illustration of Hprt-tdT Knock-in (JAX; stock# 021428) and *Pchd19* KO mice (TF2108). For *Hprt-tdT*, LSL cassette was removed by CMV-cre (top left), and for *Pchd19* KO mice, the exon 1, 2 and 3 was replaced with *β-gal/neoR* fusion cassette (top right). Two types of recombinant male mice were generated through random recombination between *Pchd19* and *tdT* genes on the same X-chromosome; $X'_{tdT}Y$(KO-tdT) and $X_{tdT}Y$(WT-tdT) (bottom).

2. Antibodies

For generation of polyclonal rabbit antibody for detecting C-terminal PCDH19, 18 amino acids of mouse PCDH19 (Lys1020-Arg1037a.a) were coupled with KLH carrier and immunized into rabbits. This antibody was characterized in both *in vitro* and *in vivo* systems. The following antibodies were commercially purchased: polyclonal rabbit antibody for neomycin phosphotransferase II (NPTII) from Millipore, polyclonal goat antibody for b-actin (C11) from Santa Cruz.

3. Real-time polymerase chain reaction (RT-PCR)

The *Pcdh19* mRNA levels from mouse brain tissue at various of developmental stages; E18.5, P7 and P14 were extracted using Hybrid-R kit (Geneall biotechnology, Seoul, Korea) and cDNA synthesized with cDNA synthesis kit (Takara bio, Shiga, Japan) and measured using RT-PCR. The expression of GAPDH mRNA served as an internal control. The RT-PCR reactions were performed with a 7500 RT- PCR System (Applied Biosystems, Foster City, CA, USA) using fluorescent SYBR Green technology (Takara bio, Shiga, Japan). Unique 18-25 bp primer pairs from coding sequences were specifically identified using Primer Express (Applied Biosystems, USA). RT-PCR was performed on 2 μl of cDNA synthesized from 200 ng of total RNA. The nucleotide sequences of two primers were used as listed below: mPCDH19, F: 5'-TGT CCT GAA CAC CAG TGT GA-3' and R: 5'- CCG AGG CAT CCA GCA TCT AT-3'; GAPDH F:5'-CCT CCT CAT GGT TGC CCT TTC-3' and R: 5'-ATG ACG AAG CCA ATC CCT GTA-3'

4. Cell culture and transfection

HEK293T, N2A, K562 (ATCC, CCL243) cells were all cultured in Dulbecco's Modified Eagle's Medium (DMEM) supplemented with 10% fetal bovine serum (FBS) and 1% PS penicillin/streptomycin (PS) antibiotics in a humidified incubator at 37°C and 5% CO_2. For transfection of HEK293T and N2A, jetPRIME (Polyplus, Illkirch, France) was used, and for transfection of primary cultured cortical neuron, was performed with lipofectamin 2000 (Life Technologies Corporation, USA) to manufacture's specifications. Cells were harvested 48hrs after transfection. For aggregation assay, 1×10^6 K562 cells were transfected with 10 μg of plasmid DNA by using Amaxa Nucleofector™ (Amaxa, Cologne, Germany) according to the manufacturer's protocol (SF cell line 4D-Nucleofector™ X Solution, program FF-120), and incubated for 24 hr.

5. Plasmids

pcDNA3-mPCDH19-GFP encodes full-length mPCDH19 cloned into pcDNA3 vector and with C-term GFP epitope inserted. pIRES2-hPCDH19-EGFP and pIRES2-hPCDH19-DsRed2 encodes full-length hPCDH19 cloned into pIRES2-EGFP and pIRES2-DsRed2 vectors using SalI and BamHI restriction sites. pCMV6-myc-DDK-hPCDH19 and pCMV6-GFP-TIMP1 were purchased (Origene, USA) Single mutagenesis was performed using pcDNA3-mPCDH19-GFP, pCMV6-hPCDH19 and pIRES2-hPCDH19-EGFP as a template to make human single nucleotide polymorphism (SNP). The detailed nucleotide sequences are shown in Table 1. All constructs were verified by sequencing.

Table 1. Mutagenesis primer sequences

Mutagenesis		
Forward sequences (5'-3')		
mPCDH19		
	L25P	CTGCCCTGATTAACCCTAAATACTCGGTCG
	D121N	GATTAAGGTGGAGATCAAAAACCTGAACGACAATGCTC
	A153T	CCCACTGGACAGTACATATGACCCGG
	F206Y	CAGTCACATTACAGCTATCGCATTACGGCTCTC
	N340S	GTCAGCGTACTTGATACTAGTGACAACCCGCCAATTATC
	V441E	CCAAGTCGTTCACTGAGCGTATCACAGATG
	L543P	GCTTGCCCTCCCCGCAAAGCAATGC
	P567L	CATCACTGCCCCACTTCTGATCAATGGC
	Q85X	CTCTTGGTCACCAAGTAGAAGATTGACCGAG
	S671X	GATGCCCAAGAGTGAATGGGCTCTGTG
hPCDH19		
	V441E	CAAGTCCTTTACCGAGCTCATCACTGACG
	N557K	CATCATCCTCGACGTCAAGGACAACACCCCGGTCATC
	T146R	AGCCCTGGCAGGCGCATCCCG
	E313K	GCACGTGTACAAACTGGACGT
	Q85X	CTGCTGGTCACCAAGTAGAAGATTGACCGTG
	S671X	CTCGATGCCCAAGAGTGAATGGGCTCTGTGAAC
Reverse sequences (5'-3')		
mPCDH19		
	L25P	CGACCGAGTATTTAGGGTTAATCAGGGCAG
	D121N	GAGCATTGTCGTTCAGGTTTTTGATCTCCACCTTAATC
	A153T	CCGGGTCATATGTACTGTCCAGTGGG
	F206Y	GAGAGCCGTAATGCGATAGCTGTAATGTGACTG
	N340S	GATAATTGGCGGGTTGTCACTAGTATCAAGTACGCTGAC
	V441E	CATCTGTGATACGCTCAGTGAACGACTTGG
	L543P	GCATTGCTTTGCGGGGAGGGCAAGC
	P567L	GCCATTGATCAGAAGTGGGGCAGTGATG
	Q85X	CTCGGTCAATCTTCTACTTGGTGACCAAGAG
	S671X	CACAGAGCCCATTCACTCTTGGGCATC
hPCDH19		
	V441E	CGTCAGTGATGAGCTCGGTAAAGGACTTG
	N557K	GATGACCGGGGTGTTGTCCTTGACGTCGAGGATGATG
	T146R	GGCTGCCTCCGAGATCTCCAG
	E313K	CCCTCTTCGTAGTCTAAAG
	Q85X	CACGGTCAATCTTCTACTTGGTGACCAGCAG
	S671X	GTTCACAGAGCCCATTCACTCTTGGGCATCGAG

6. Drugs

Secretase inhibitors; N-[N-(3,5-difluorophenavetyl)-L-alanyl] -(S)-phenylglycin t-butyl ester (DAPT; Tocris, UK) and GI254023X (GI; Tocris, UK) were dissolved in DMSO solution. To evaluate the effect of secretase activities, 50 uM DAPT or DMSO (vehicle) treated before 24 hr and 10 uM GI treated before 30 min in *in vitro* experiments. For *in vivo* experiments, P7 WT mice received systemic treatment with the ADAM10 inhibitor GI (80mg/kg/day) or DMSO (vehicle) for 3 consecutive days from P7 to P9 by intraperitoneally (i.p.) injection and brain was isolated at P10 (Figure 2). Pilocarpine hydrochloride (P5603, Sigma Aldrich, USA) and scopolamine methyl bromide (S8502, Sigma Aldrich, USA) were both dissolved in sterile 0.9% NaCl to make 10 mg/ml and 0.5 mg/ml respectively.

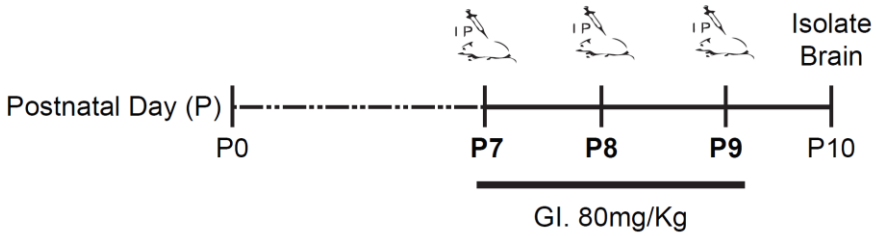

Figure 2. *In vivo* administration schedule of a ADAM10 inhibitor, GI254023X (GI). From postnatal day 7 (P7), mice were administrated with 80 mg/kg of GI or vehicle (DMSO) once a day by i.p. injections. At P10, brain sample was isolated for protein analysis.

7. Pilocarpine-induced seizure model

Pilocarpine is a non-selective agonist of muscarinic (M) receptor that activates M1 receptor, generating an imbalance between excitatory and inhibitory synaptic transmission in turn, causing seizure.[23,24] All genotypes of *Pcdh19* KO mice received 2 mg/kg scopolamine methyl bromide intraperitoneally 30 min before administration of pilocarpine injection to avoid any peripheral cholinergic effects of pilocarpine drugs. All mice were aged between 12-13 weeks old were tested for seizure susceptibility by pilocarpine injection. The time taken to show first seizure like behaviour was defined as latency to clonus, and the latency to generalized seizure (tonic-clonic, whole body seizure) were also monitored. 500 mg/kg and 300 mg/kg of pilocarpine was injected to female mice (XX, XX' and X'X') and male mice (XY and X'Y) respectively. For female, n=13-16 mice and for male n= 5 per genotypes were used (Figure 3).

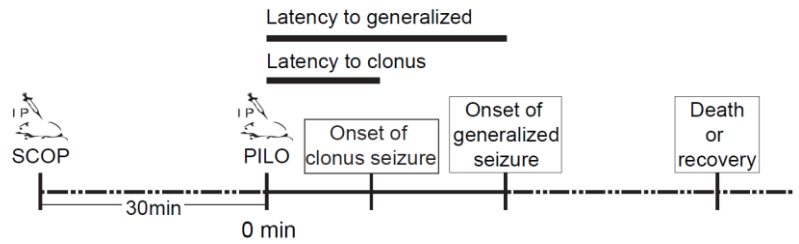

Figure 3. A schematic of pilocarpine-induced seizure. Mice were intraperitoneally injected with scopolamine methyl bromide (SCOP) 30 min before pilocarpine hydrochloride (PILO) injection. The latency to clonus and generalized seizure were calculated from the time of PILO injection (0 min), not SCOP.

8. Whole brain lysate and crude synaptosomal fraction preparation

Mice brains were briefly homogenized in ice-cold homogenization buffer (0.32 M sucrose, 5mM HEPES, 1mM EDTA, pH 7.4) containing protease inhibitor cocktail tablet (Roche, Basel, Switzerland), centrifuged at 1,000 g for 10-min at 4°C. Only the supernatant was collected for whole brain lysates, then lysis buffer (50 mM Tris-HCl, 150 mM NaCl, 1% Triton X-100, 0.1% SDS, 2 mM EDTA) containing protease inhibitor cocktail tablet were added and rotated at 4°C for 30-min. Then centrifuged again at 12,000 g for 20-min at 4°C, supernatant from this is used as whole brain lysate. For crude synaptosomal fraction preparation, half of homogenized lysates are re-centrifuged at 12,000 g for 20-min at 4°C. This time, supernatant had been discarded and pallets were resuspended in lysis buffer.

9. Surface biotinylation and immunoblotting

After 48 hr of transfection, HEK293T cells were washed three times with cold PBS on ice. The surface membrane proteins were then biotinylated with buffer that contains 0.3 mg/ml EZ-link Sulfo-NHS-SS-Biotin (Pierce, Rockford, IL, USA) for 30 min at 4°C. Cells were washed three times with cold PBS then incubated 10 min on ice with quenching buffer of 1% BSA solution to quench unreacted biotin. Cells were washed twice with PBS, then lysed with Lysis buffer (20 mM Tris-HCl, 150 mM NaCl, 5 mM EDTA, 5% glycerol, 1% Triton X-100) containing protease inhibitor cocktail tablet (Roche, Basel, Switzerland). Cell lysates were centrifuged at 13,000 rpm for 20 min. 15% of the supernatant was saved as the total protein lysate. The supesrnatant was incubated with 20% diluted streptavidin agarose beads (Pierce,

Rockford, IL, USA) for overnight at 4°C. The concentration of protein was determined by using BCA protein assay kit (Pierce, Rockford, IL, USA). Next day, Avidin-biotin bound complexes were pelleted and washed three times with lysis buffer. Biotinylated proteins were eluted in 5X sample buffer at 37°C for 1 hr, resolved by SDS-PAGE and transferred onto polyvinylidene fluoride (PVDF) membranes. The membranes were blocked with 5% milk in TBS-T (0.05% Tween20) for 1 hr, and incubated overnight at 4°C with PCDH19 (1: 1,000), β-actin (1: 1,000, sc1615, Santa Cruz Biotechnology), NPTII (1: 1,000, Millipore) primary antibody. The membranes were washed three times with TBS-T for 10 min, then was incubated with horseradish peroxidase-conjugated anti-rabbit, anti-goat secondary antibody (1: 5,000, Thermo scientific, Waltham, MA, USA) for 1 hr at room temperature. The immune-reactive bands were visualized with ECL chemiluminescence reagent (Thermo scientific, Waltham, MA, USA), then scanned.

10. Brain dissection

Mice were decapitated under deep anesthesia; the brain was quickly removed. Whole brain was isolated from cranial and immediately frozen in liquid nitrogen for preparation of whole brain lysate. For dissecting different regions, the brain was carefully placed onto a petri-dish with ice-chilled PBS. Six brain regions were dissected rapidly: Cortex, hippocampus, cerebellum, basal ganglia, brain stem and spinal cord. Dissected samples were put into cryotube (Nunc, Roskilde, Denmark) and immediately frozen in liquid nitrogen, and stored in a liquid nitrogen tank until day of protein preparation

11. Embryo brain preparation and immunohistochemistry

For embryo brain preparation, females were inspected daily for vaginal plugs as an indication that copulation had occurred (day 0.5 of pregnancy) to calculate embryonic days. The embryonic brain was carefully placed onto petri-dish with ice-chilled PBS under dissection microscopy and fixed with 4% paraformaldehyde for overnight at 4°C cryoprotected in 30% sucrose, then embedded in OCT compound (Cellpath, Mid Wales, UK) and frozen. All embryonic brains were cut into 12μm coronal sections on cryostat (Leica biosystems, Buffalo Grove, IL, USA). The slide with sections were washed once with PBS for 10 min at room temperature, and mounted using Vectashield with DAPI solution (Vectorlab, Burlingame, CA, USA). Slides were observed under Axio Image M2 (Gena, Germany).

For immunohistochemistry of *Pcdh19* KO mice adult brain, brain samples were cut into 50 um coronal sections using vibratome (VT1200S, Leica Nussloch, Germany) after fixed with 4% paraformaldehyde for overnight at 4°C. Sections were blocked and permeabilized with 2% BSA with 0.4% Triton X-100 in PBS for 1 hr at room temperature. Afterward, they were incubated with the Parvalbumin, (1: 50, Swant, PVG213) in 1% BSA with 0.1% Triton X-100 for overnight at room temperature. Sections were washed three times with PBS for 10 min, then incubated with 1: 1,000 dilution of Alexa 488 conjugated donkey-anti-goat antibody and DAPI (1: 2,000, Sigma Aldrich, St Louis, MO, USA) for 1 hr. Sections were washed three times and mounted with Flouromount-G (OB100-01, Southern biotech, Birmingham, Alabama, USA). Slides were observed under Axio Image M2 (Gena, Germany).

12. Cell aggregation assay

Cell aggregation assays were performed with K562 cells as described previously[25] with minor modifications. K562 cells were transfected with pIRES2-hPCDH19-EGFP (WT) or pIRES2-hPCDH19-DsRed2 (WT) or pIRES2-hPCDH19 (V441E/N557K/T146R/E313K)-EGFP (mutant-type) expression plasmid with Amaxa Nucleofector™ as mentioned in transfection method section. After 24 hr, transfected K562 cells were harvested, pelleted and resuspended in HCMF buffer (137 mM NaCl, 5.4 mM KCl, 0.34 mM Na_2HPO_4, 5.5 mM glucose and 10 mM HEPES, pH7.4) with DNase (10 μg/ml). In order to obtain a single cell suspension, cells were passed through a 40 μm cell strainer (Falcon), and 1 X 10^5 total cells (0.5 X 10^5 per sample in heterogeneous condition) were added to each well of 24 well cell-culture plate (Falcon) with Ca^{2+} solution (HCMF/50 mM HEPES and 10 mM $CaCl_2$) or without Ca^{2+} solution as a control (Ctl: HCMF/50 mM HEPES only). Then, they were incubated to aggregate for 1, 3, 5 and 8 hrs on a nutator with gentle agitation at 37°C and 5% CO_2. Aggregated cells were imaged using a Nikon Eclipse Ti-U microscope (Tokyo, Japan). For quantification, TIFF images were analyzed using Image J, where they were subjected to equal threshold and then analyzed with "analyze particle" function. Particle size from 4 biological repeats were used in this quantification and the particle size below 150 pixels were removed because it was considered as background particles.

13. Rat primary neuron culture

Rat primary neuron culture was prepared as described in details previously.[26] Briefly, embryonic 18 days (E18), embryos were removed surgically from anaesthetized pregnant SD rat, which was purchased from Orientbio Inc. (Seongnam, Korea). The fetal rat brain was dissected in cold dissection medium (DM; HBSS with 1% PS and HEPES) under a microscope. The pia matters with meninges, blood vessels were removed, and part of cortex were collected. Collected tissues were treated with 0.25% trypsin in DM at 37 °C for 15 min, and triturated with a Pasteur pipette. Pelleted cells were diluted to a concentration of 5×10^4 cells/mL in neurobasal medium with 100X glutamax and B-27 supplement for imaging. These suspended cells were placed in a Poly-D-Lysine coated 12 mm cover-glass (Germany), and half of the media were changed every 3-4 days and neurons were fixed at DIV 7 and 14.

Cultured neurons were fixed with removing half of the growth medium and adding half volume of 4% paraformaldehyde (PFA), 4% sucrose solution (final of 2% PFA and sucrose) for 2 min. Then, the pre-fixed medium was replaced to a fresh 2% PFA and 2% sucrose solution and incubate for 20 min at room temperature. This was necessary to minimize the damages of the neuronal processes. To observe the overexpressed PCDH19 cellular localization, the cortical neurons were transfected each with hPCDH19-EGFP or hPCDH19(V441E)-EGFP constructs at DIV 5 and DIV 12. Imaged were acquired using a confocal microscope LSM710 (Carl Zeiss, Germany).

14. Statistical analysis

Statistical significance was determined using One-way analysis of variance (ANOVA) followed by Turkey, Bonferroni *post hoc* test for multiple comparisons between groups. For aggregation quantification, the averaged particle sizes were then compared to Ctl (no Ca^{2+}) using Kruskal-Wallis test followed by Dunn's multiple comparison were performed using GraphPad Prism 7 software (GraphPad Software, Inc., La Jolla, CA, USA). Values $p < 0.05$ were considered statistically significant.

III. RESULTS

Part1:

1. The expression patterns of PCDH19 during mouse brain development

Previous *in situ* hybridization analysis has demonstrated that PCDH19 is predominantly expressed in neural tissues and at different developmental stages.[8,22,27] Since there are no commercially available KO validated PCDH19 antibodies, we first generated the C-terminus anti-mPCDH19 antibody to analyze the expression of endogenous PCDH19 protein. Protein expression of endogenous PCDH19 in the whole brain lysate of both adult male and female mice were analyzed through western blot assay using this C-terminus PCDH19 antibody. The ~135 kDa band was present in the WT mice and the expression level of PCDH19 was reduced in the female HET, but absent in both male and female *Pcdh19* KO mice (Figure 4A). Taking the advantage of the KO validated antibody, I investigated the expression of PCDH19 in various regions of the mouse brain at different developmental stages from embryonic day18 (E18) to postnatal day56 (P56) (Figure 4B). PCDH19 was expressed in almost all regions of the brain and its expression levels gradually increased during the early developmental stages in which peaked around P7 and dropped dramatically after this time point (Figure 4C). Although PCDH19 expression were dramatically decreased after P7, robust protein expression was constantly seen in the cortex and hippocampus both in developing (P7) and adult (P56) brains (Figure 4D), which is consistent with previously reported mRNA expression data.[8] Nonetheless, the PCR analysis showed no significant changes in the mRNA levels between P7 and P14. This clearly indicates that the significant decline in PCDH19 protein expression observed after P7 was not

due to the decrease in mRNA transcription levels (Figure 4E), suggesting this decay phenomenon is more likely to be regulated by post-transcriptional modulation. Therefore, I can speculate that the physiological role of PCDH19 is important, especially during early brain development. The rising phase of PCDH19 expression during early brain development overlaps with the time course of critical neuronal development, such as neuronal circuitry, synapse formation and migration, and any disruptions of these are closely related to induce epilepsy.[28]

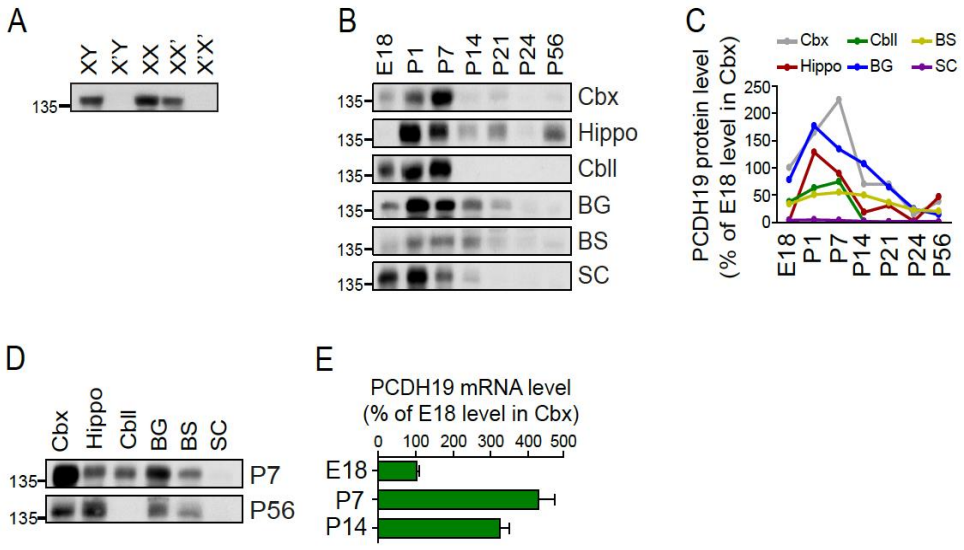

Figure 4. Developmental changes of PCDH19 expression patterns in the mouse brain. A. Western blot analysis of PCDH19 protein in the whole brain lysate from different genotypes of adult *Pcdh19* KO mice model. The anti-mPcdh19 C-terminus antibody detects a ~135kDa protein in WT (XY, XX) and heterozygous mutant (XX') and disappears in *Pcdh19* KO (X'Y, X'X') mice. B. Expression of PCDH19 in lysates of different brain regions of mouse brain (Cbx, cortex; Hippo, hippocampus; Cbll, cerebellum; BG, basal ganglia; BS, brain stem; SC, spinal cord) at different embryonic (E) and postnatal (P) days. C. Relative quantification of PCDH19 expression to Cbx expression level at E18. D. Relative PCDH19 expression levels of different brain regions of mouse brain at P7 (young) and P56 (adult). E. RT-PCR results of PCDH19 mRNA levels of the mouse brain at different developmental time points (E18, P7, P14). PCDH19 mRNA fold changes of PCDH19 mRNA were compared to the fold of Cbx E18. All data are presented as means ± s.e.m.

2. Characterization of EFMR-causing mutation of PCDH19

To date, more than 145 different disease causing PCDH19 mutations (271 cases) have been reported in EFMR patients, approximately 45% are missense mutations, 27% are frameshift, and 20% are nonsense mutations.[29] Although many genetic variants were frequently reported, the cellular and molecular mechanisms related to these mutations are still poorly understood. I have selected several EFMR-causing mutations (both nonsense and missense) in *PCDH19*, previously reported through familiar pedigree studies,[8] which are distributed throughout all six extracellular cellular domains (Figure 5A). Cell surface biotinylation assay was conducted using HEK293T cells that express several missense-mutant and WT of *Pcdh19*, and showed increased expression levels in some of the missense mutations compared to the WT (Figure 5B). Dibbens et al. (2008) first reported several nonsense and missense mutations in families with EFMR.[8] Since nonsense mutations give rise to premature termination of PCDH19 translation, western blot analysis of HEK293T cell transfected with nonsense *Pcdh19* mutations showed no protein expression in both 253C>T (Q85X) and 2012C>G (S671X) mutations (Figure 5C). Also, western blot analysis of *PCDH19* demonstrated the same abolished expression of nonsense-mediated *PCDH19* mutations (Figure 6A, B). Moreover, two missense mutations of *PCDH19*; 1322T>A (V441E) and 1671C>G (N557K) showed increased surface expression levels compared to the WT (Figure 6A, C). This suggests that some missense and nonsense mutations of PCDH19 would act distinctively in causing EFMR and gives rise to the possibilities that some of the missense mutations are gain of function mutations by increasing the level of cell surface proteins.

Generally *PCDH19* is located in the cell membranes and undergoes calcium dependent hemophilic interactions at the cell surface.[30] DNA construct of *EGFP* conjugated at the C-terminus of *PCDH19*-WT was transfected in rat primary cultured cortical neurons to investigate the role of PCDH19 in neurons. Transfected *PCDH19*-WT-*EGFP* signal was observed outside the nucleus in an early developing neurons of day *in vitro* (DIV) 7 (Figure 6D, left above) and then *EGFP* signal was translocated to the nucleus as neurons matured at DIV14 (Figure 6D, right above). However, *EGFP* signal of the V441E mutation was absent from the nucleus of neurons at both DIV7 and 14 (Figure 6D, below). This change in localization of PCDH19 during neuronal development in primary cultured neurons lead me to the idea that PCDH19 might undergo a proteolytic cleavage pathway, similar to other adhesion molecules within the cadherin families such as N-cadherin and E-cadherin that are important in neuronal development.[31-33]

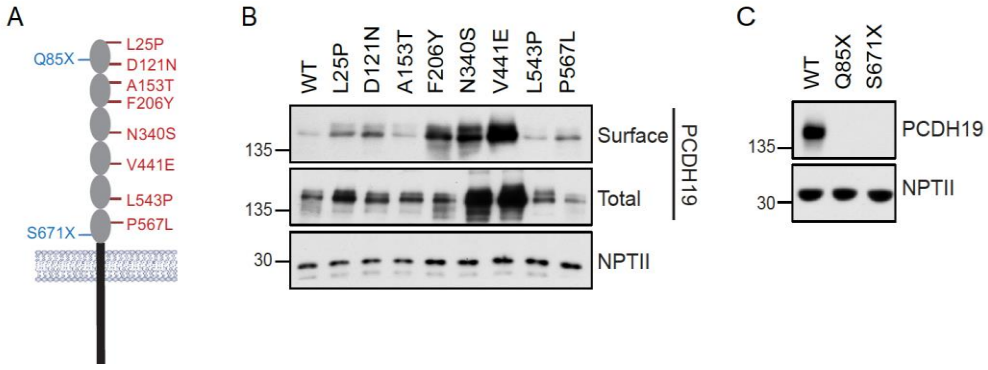

Figure 5. Characterization of EFMR-causing mutations of PCDH19. A. Schematic diagram of PCDH19 molecule with various mutation sites are listed on extracellular domains (EC1-6), nonsense mutations on the left, missense mutations on the right side. B. Cell surface biotinylation expression *PCDH19*-WT and several EFMR-causing missense mutations, using *PCDH19*-GFP transfected HEK293T cells. C. Cell surface biotinylation expression WT and several EFMR-causing nonsense mutations, using *PCDH19*-GFP transfected HEK293T cells.

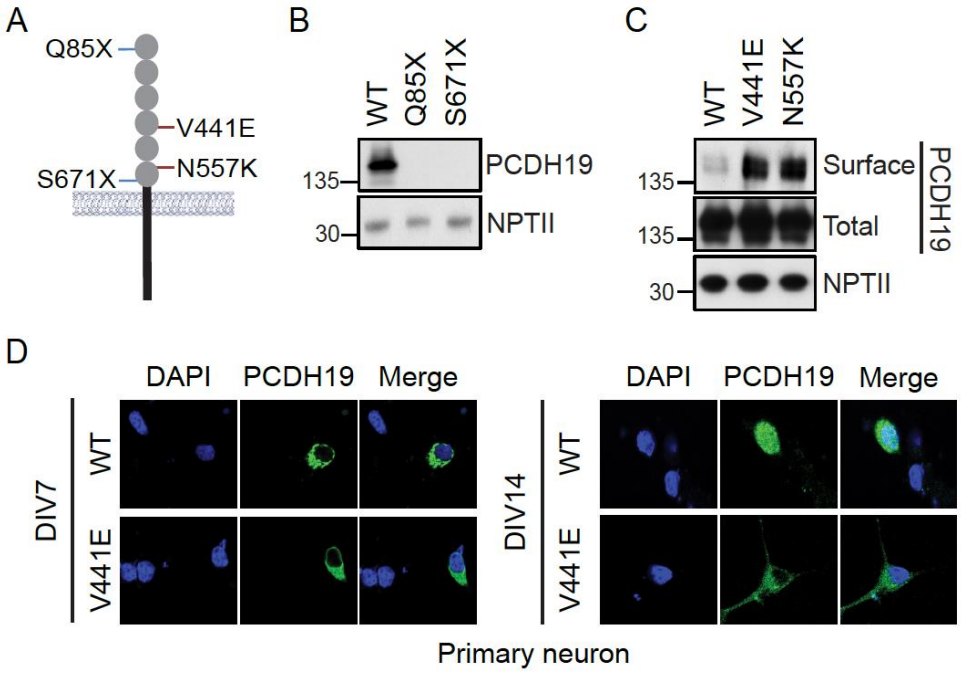

Figure 6. Characterization of V441E missense mutation. A. Schematic diagram of PCDH19 with mutations identified through the study of previous genetic pedigrees of the EFMR families, along extracellular domains (EC1-6). Two nonsense mutations marked on the left, two missense mutations on the right side. B-C. Western blot analysis of surface biotinylation of HEK293T cell with PCDH19-WT and missense (B) and nonsense (C) mutations. D. Nuclear translocalization of PCDH19 proteins during neuronal maturation, using primary cultured rat cortical neurons which were transfected with either PCDH19-WT-EGFP or PCDH19–V441E-EGFP mutation.

3. PCDH19 undergoes a proteolytic cleavage pathway

A molecular mechanism of regulated intramembrane proteolysis (RIP) is essential in cell-cell interaction.[34] Typically, two consecutive proteolytic cleavages happen in the RIP process via metalloproteinase and γ-secretase action. The first cleavage occurs at the extracellular (EC) domain via α, β -secretases, then γ-secretase sequentially cleave the transmembrane (TM) domain, releasing the intracellular (IC) domain into the cytosol.[35,36] HEK293T cells expressing PCDH19-WT and PCDH19-V441E were treated with ADAM10 (A disintegrin and metalloproteinase 10) inhibitor; a component of α-secretase, GI, and the γ-secretase complex inhibitor, DAPT. The surface protein expression of the GI-treated PCDH19 WT group showed increased expression of PCDH19, but not in the DAPT treated group compared to non-treated WT (negative) group (Figure 7A). Since the action of α-secretase has been inhibited by GI treatment, EC domain of the surface PCDH19 was "un-cleaved" hence, the expressions of PCDH19 were elevated in the western blot assay. Although γ-secretase were blocked by DAPT treatment, EC domains of PCDH19 had already been cleaved by α-secretase therefore, this resulted in unchanged expression levels of PCDH19 compared to the WT (negative) group. Meanwhile, the surface expression level of PCDH19 in V441E group was already higher than WT (also in Figure 6C), the expression levels did not change in neither of the GI- and DAPT-treated groups (Figure 7A). To investigate the effect of endogenous inhibitors of metalloproteinases, both PCDH19-WT and -V441E were co-transfected with TIMP-1 (tissue inhibitor of metalloproteinases). TIMP-1 and WT co-transfected cells also increased PCDH19 protein expression, but not in the TIMP-1 and V441E co-transfected group (Figure 7B). Additionally, the disturbance of translocalization to the nucleus was also shown

in GI-treated group of PCDH19-WT transfected Neuro2A (N2a) cells (Figure 7C), which was similar to the results of the V441E-transfected primary cultured neurons in Figure 6D. To ensure the secretase activity associated with cellular localization of PCDH19 can be demonstrated *in vivo*, GI (80 mg/kg/day) or DMSO (vehicle) was injected into the mice for 3 consecutive days starting from P7. Consistent with *in vitro* findings, PCDH19 protein levels were significantly increased in the GI-injected group compared to DMSO-injected group in the crude synaptosomal fractions (Figure 7D-F). These data strongly support that PCDH19 proteins are modulated through the secretase dependent cleavage pathway. However, missense-mutant PCDH19 are resistant to normal proteolytic cleavage, accumulating abnormal proteins at the cell surface that should normally be processed. This may provide a novel insight to understand the pathophysiology of EFMR.

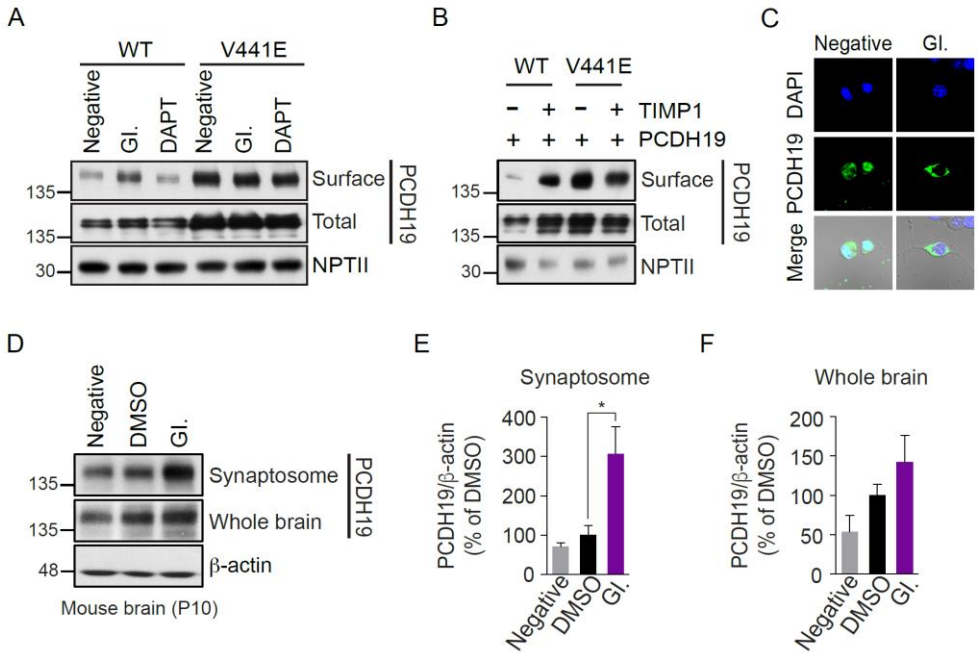

Figure 7. V441E missense mutations of PCDH19 inhibit secretase-dependent C-terminal cleavage process in both *in vitro* and *in vivo*. A. Surface biotinylation assays of HEK293T expressing PCDH19-WT and PCDH19-V441E were treated with secretase inhibitors GI and DAPT. B. Surface biotinylation assays of co-transfected TIMP1 with PCDH19-WT or PCDH19-V441E. C. Overexpression of PCDH19-WT on Neuro2A cells treated with secretase inhibitor, GI. D. Western blot analysis of crude synaptosomal and whole brain lysates of GI (80 mg/kg/day, i.p.) and vehicle (DMSO) injected mice brain at P10 (I.P injection from P7 to P9). E-F. Relative quantification showing the percentage of PCDH19 expression of crude synaptosomal and whole brain fractions. All groups were normalized to actin and then divided by DMSO injected group as control. One-way ANOVA, Turkey *post hoc* test, $*p < 0.05$. All data are presented as means ± s.e.m.

4. The adhesive properties of PCDH19 wild-type and different PCDH19 missense mutants

Neuronal architecture is essential in the development of vertebrate nervous system, and cell-cell recognition plays a central role in establishing functional neural circuit development.[37,38] E-cadherin was the first identified protein that mediates calcium dependent cell-cell adhesion.[39] Then, other cadherin families have been characterized to play a crucial role in the formation and maintenance of tissue architecture through their calcium dependent adhesion activities of their extracellular cadherin repeat, one of the well-known example is N-cadherin.[40] Protocadherins are the largest cadherin superfamily and they are expressed in the developing nervous system, most of them enhance a homophilic cell aggregation. Although, the cell-cell adhesion mediated by protocadherins are weaker than the cadherin-mediated ones, it is still crucial in diverse signaling functions, especially in the neural circuitry development.[41] PCDH19 is a member of the non-clustered δ2-protocadherins.[6,10] Dysfunction of these non-clustered δ-protocaherins are associated with neurological diseases like autism spectrum disorders, intellectual disability, and epilepsy.[7-9] Despite the clear importance of the role of non-clustered δ-protocaherins, they are only beginning to be discovered. Non-clustered δ-protocaherins mediates cell-cell adhesion through homophilic interactions[15,42,43] however, the adhesive functions of PCDH19 is still not fully understood. Since the adhesive properties of PCDH19 are still relatively vague, prior to perform calcium dependent cell-cell aggregation assay using PCDH19 molecule, *E-cadherin-EGFP* expressing K562 cells were used as a positive control in the cell aggregation assay. As expected, E-cadherin efficiently form cell aggregates in a 1 hr of incubation period in the presence of calcium (Figure

8A-B). Recently, several EFMR-causing missense mutations were shown to abolish its adhesive functions,[11,16] which provides a similar molecular basis as nonsense mutations to understand EFMR. Before proceeding the cell aggregation assays using different PCDH19 missense mutant-expressing cells, I firstly needed to find the optimal condition for PCDH19–WT cells to aggregate. Different incubation periods; 3, 5 and 8 hrs were tested with K562 cells expressing PCDH19-WT and found that 8 hr of incubation period produces the most sufficient amount of cell aggregates in the presence of calcium in this experiment (Figure 9A-C). It is obviously noticeable that PCDH19 displayed much weaker adhesive abilities than E-cadherin. Therefore, PCDH19-WT was shown to be a surface adhesion molecule that mediates homophilic adhesion. Then, several EFMR-causing missense mutants were tested as well as PCDH19-WT (Figure 10-11). Two missense mutations, V441E and N557K (group 1), showed similar aggregate affinity to WT (Figure 10A-C). When cells expressing theses PCDH19 mutants were mixed with cells expressing DsRed2-conjugated PCDH19-WT to mimic the cellular mosaic composition seen in EFMR, abnormally augmented cell aggregates were formed in the presence of calcium (Figure 10D-F). Then I have tested some other missense mutations (T146R and E313K) that were previously reported to lack its adhesive functions,[11] and obtained the similar results as previously reported (Figure 11). Because it showed loss of adhesive function in a homogeneously mixed condition (Figure 11A-C), it failed to form any cell aggregates even when it was mixed with WT in a heterogeneous condition (Figure 11D-F). Recently, PCDH19 adhesion is mediated by a antiparallel homophilic *trans*-interactions of fully overlapping EC1 to EC4 domains, which is the binding structures for clustered PCDH family.[11,44] Clustered PCDH family formed heterotypic *cis*-interaction with other non-clustered PCDHs that induces cell sorting because they

generate specific binding affinity.[16] This antiparallel interaction structural model of PCDH19 is only suitable to explain the previous hypothesis that all missense mutations are loss of function of the protein. Previously, missense mutations along the extracellular domains of PCDH19 interfere with the Ca^{2+} binding site and attribute to loss of their adhesive activities within the EC1 to EC4 domains in causing EFMR. However, this structural model does not support the phenomenon I observed in the cell aggregation assay, therefore I came up with the new dimer-antiparallel structural hypothesis. Using this model, some missense mutations of PCDH19 that showed atypical adhesive activities when mixed with WT expressing cells can be explained. Missense mutations could be sub-grouped into group1 and 2, depending on the location of the mutation sites within EC domains that could be normally regulated by secretase activities. When a missense mutation in one of the EC domains occur, it blocks the normal secretase functions to cleave, thus increases the un-cleaved proteins on the cell surface. This high expression of mutant-PCDH19 proteins can functionally alter their normal adhesive functions. Assuming that PCDH19 exist in dimer form connected with *cis*-bonds in between, homogeneous interaction of PCDH19-WT to WT needs at least 4 connected EC domains with *trans*-bonds to form cell aggregates (Figure 12B). For group 1 missense mutations; V441E on EC4 and N557K on EC5, considering their mutation sites, there are at least two consecutive *trans*-bonds between EC2 and EC3 and as well as sufficient amount of *cis*-bonds. This allows mutations to have similar adhesion affinity to WT in the homogeneously mixed conditions (Figure 12C). However, for group 2 missense mutations; T146R on EC2 and E313K on EC3, non-sequential *trans*- and not enough *cis*-bonds are formed. This induces each molecule units to dissociate and consequently abolish their adhesive activities (Figure 12D). In heterogeneously mixed condition with WT cells, where

WT-PCDH19 aggregates are nearby, unstably bonded aggregates of group 1 mutations could attract WT aggregates to compensate for their instability that will lead to form abnormal size of cell aggregates as a result (Figure 12E). There are inadequate number of *trans*- and *cis*-bonds for group 2 mutations, thus mutation units are dissociated again, fail to form any aggregates despite the presence of PCDH19-WT aggregates (Figure 12E). The distinctive adhesive properties of different missense mutations of PCDH19 could be determined by whether it undergoes secretase-dependent cleavage or not. Accumulation of 'un-cleaved' mutant PCDH19 on the cell surface could attract available WT aggregates in mosaic conditions further provides a clue to understand how missense mutations lead to pathophysiology of EFMR.

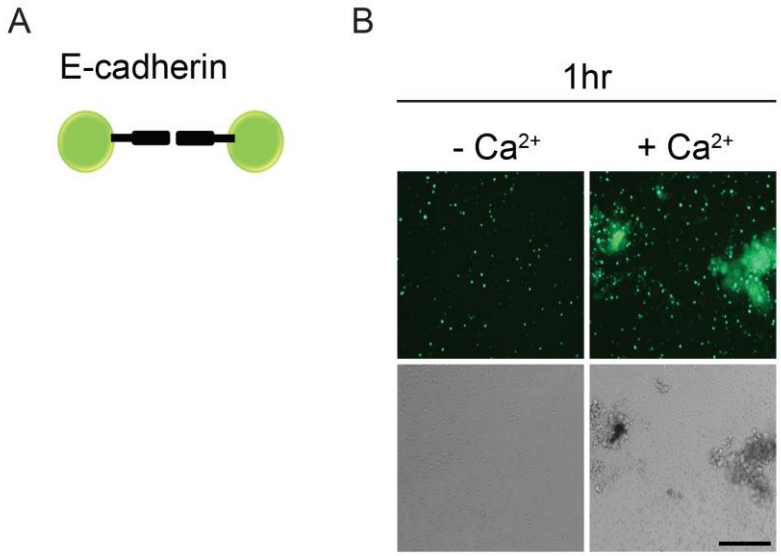

Figure 8. C**ell aggregation assay with E-cadherin-expressing cells in the presence of external calcium.** A. Schematic diagram of the cell aggregation assay of EGFP conjugated E-cadherin-WT constructs only. B. K562 cells expressing E-cadherin-WT form cell aggregates in the presence of calcium after a 1 hr incubation. Scale bar = 200 μm.

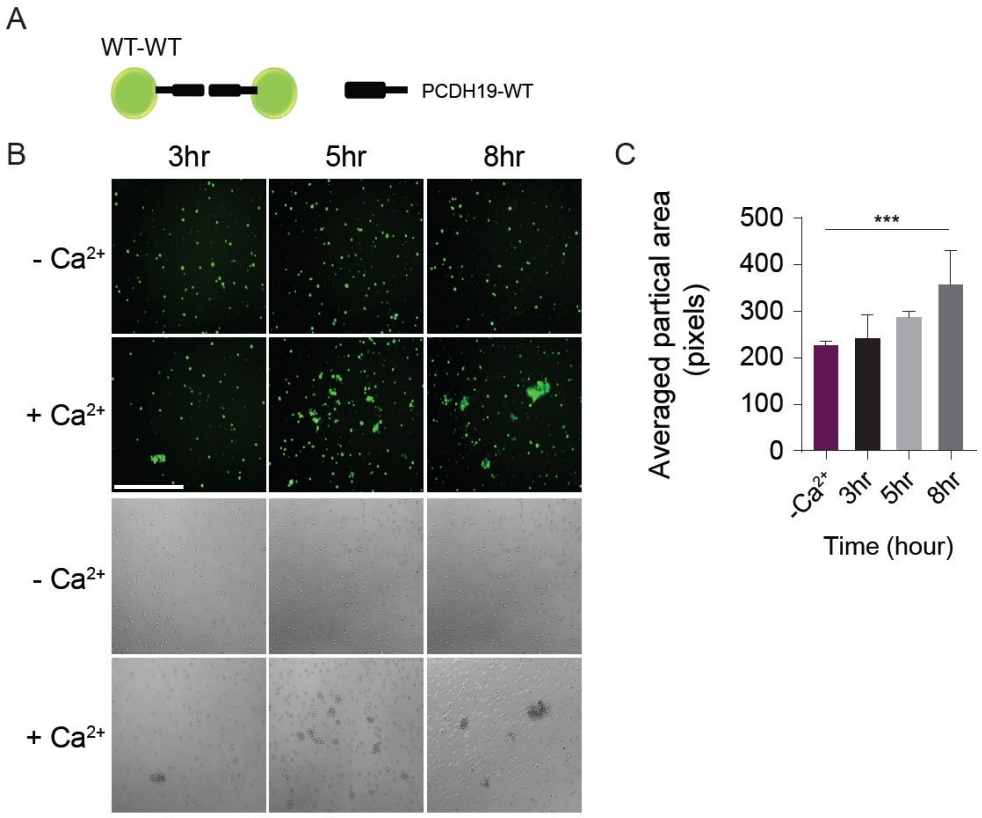

Figure 9. Cell aggregation assay with PCDH19-expressing cells in the presence of external calcium at different incubation periods. A. Schematic diagram of the cell aggregation assay of EGFP conjugated hPCDH19-WT construct only. B. K562 cells expressing hPCDH19-WT form cell aggregates in the presence of Ca^{2+} depending on various of incubation periods (3, 5 and 8 hrs). Scale bar = 200 μm. C. Quantification of averaged aggregate particle area showing 8 hr incubation was most sufficient. Kruskal-Wallis test followed by Dunn's multiple comparison test (***$p <$ 0.001). All data are presented as means ± s.e.m.

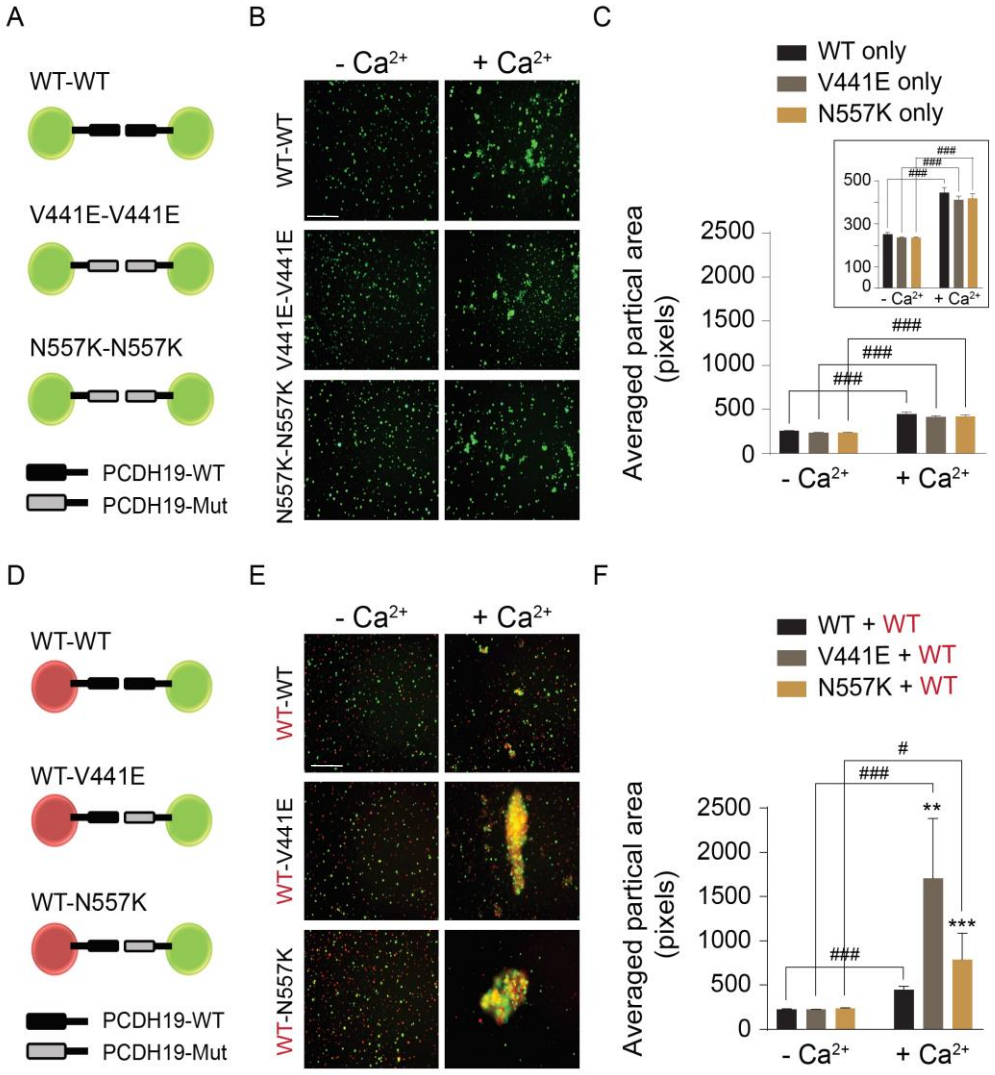

Figure 10. Identification of a group of EFMR-causing missense mutations that formed abnormally augmented cell aggregates in the artificial mosaic environment, where some PCDH19-mutant expressing cells are mixed with WT cells in the mixing cell aggregation assay. A. Schematic diagram of the cell aggregation assay of hPCDH19-WT-EGFP or few missense mutations; V441E or N557K only. B. K562 cells expressing PCDH19-WT or either one of the missense

mutations-EGFP (V441E or N557K) form cell aggregates in the presence of calcium. C. Quantification of averaged aggregate particle area in the presence of external calcium (Inset graph; different scale of y-axis). Kruskal-Wallis test followed by Dunn's multiple comparison test (###$p < 0.001$). D. Schematic diagram of the cell aggregation assay which represent hPCDH19-WT-DsRed2 mixed with few hPCDH19-missense mutations-EGFP; V441E or N557K to mimic mosaicism seen in EFMR. E. Increased number of abnormally augmented cell aggregates forming when K562 cells expressing PCDH19-WT-DsRed2 and either one of the EGFP expressing missense mutations (V441E or N557K) were mixed together in comparison to WT-EGFP mixed group in the presence of 10 mM calcium. Scale bar = 200 μm. F. Quantification of averaged aggregate particle area in the presence of external calcium. Kruskal-Wallis test followed by Dunn's multiple comparison test (#$p < 0.05$, ###$p <$ 0.001, **$p < 0.01$, ***$p < 0.001$). Data are presented as means ± s.e.m.

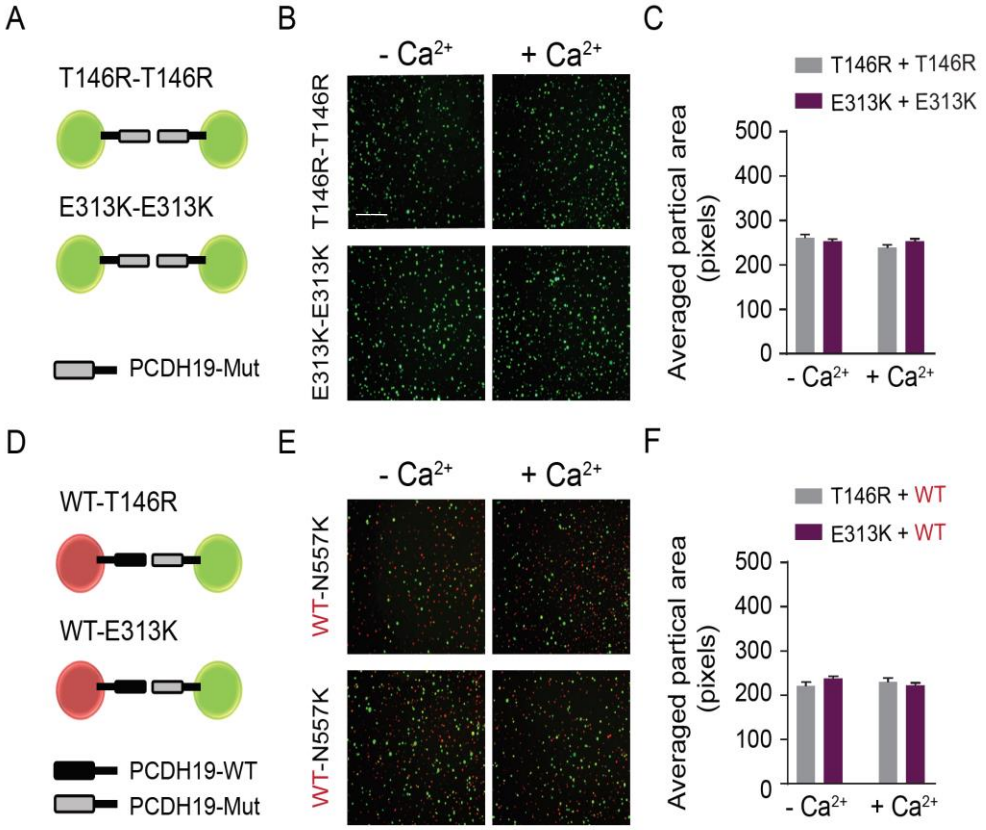

Figure 11. Identification of a group of EFMR-causing missense mutations that are loss of adhesive function in the mixing cell aggregation assay. A. Schematic diagram of the cell aggregation assay of some missense mutations hPCDH19-T146R-EGFP and hPCDH19-E313K-EGFP alone. B. K562 cells expressing some missense mutations-EGFP (T146R or E313K) fail to form cell aggregates in homogeneous condition in the presence of 10mM calcium. C. Quantification of averaged aggregate particle area in homogeneous condition. D. Schematic diagram of the cell aggregation assay of some missense mutations hPCDH19-T146R and -E313K each mixed with DsRed2 expressing hPCDH19-WT construct. E. K562 cells expressing some missense mutations (T146R or E313K) fail to form cell aggregates in heterogeneous

(each mutation combined with WT-DsRed2) conditions in the presence of 10 mM calcium. F. Quantification of averaged aggregate particle area in heterogeneous conditions. Data are presented as means ± s.e.m.

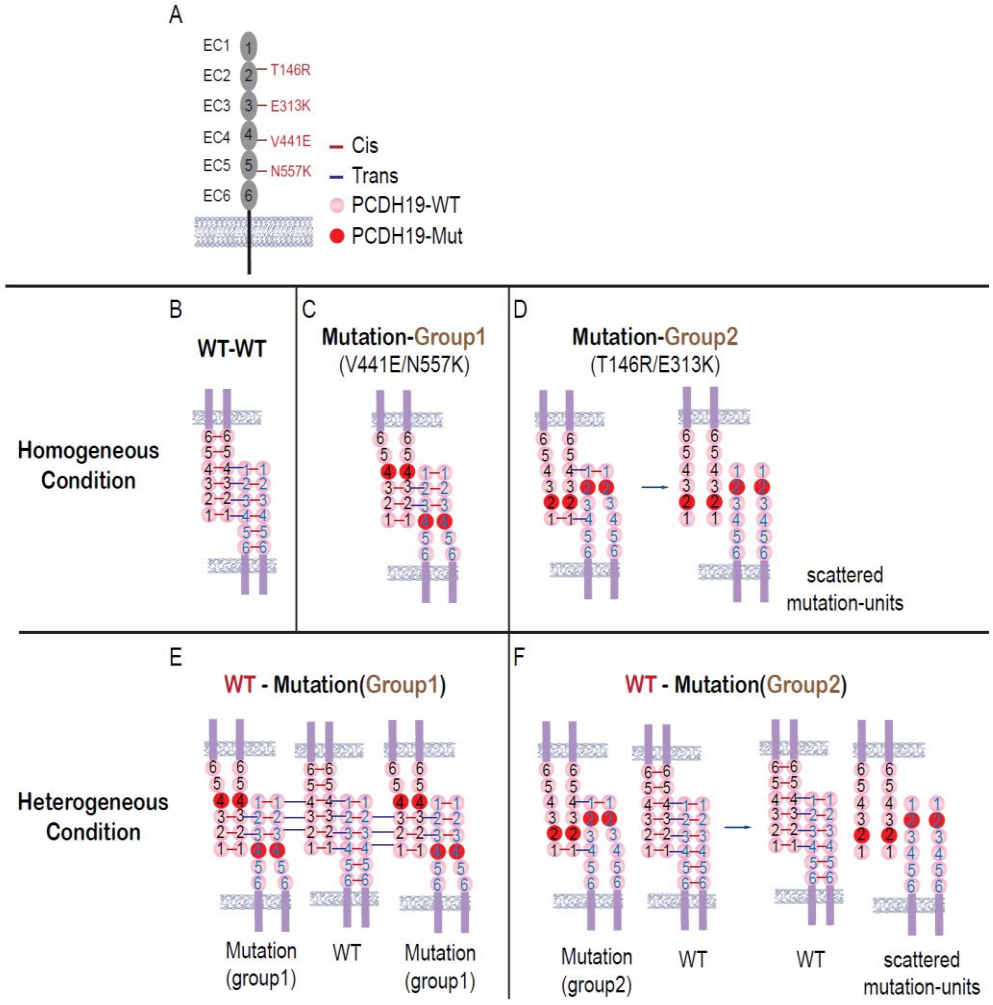

Figure 12. Modified schematics of previously proposed homophilic 'forearm handshake' models representing different adhesive characteristics of PCDH19 and the missense mutations. A. Schematic diagram of PCDH19 molecule with four different missense mutations of the EFMR, along extracellular domains (EC1-6). Red line: *cis*- bond, blue line: *trans*-bond, pink circle: PCDH19 WT, red circle: PCDH19 missense mutation. B-D. Homogeneously mixed condition; B. PCDH19-WT. C. Mutation-group1; V441E-V441E or N557K-N557K. D. Mutation-group2; T146R-

T146R or E313K-E313K. E-F. Heterogeneously mixed condition; E. Mutation-group1; WT-V441E or WT-N557K. F. Mutation-group2; WT-T146R or WT-E313K.

Part2:

5. Mosaic expression of PCDH19 exhibits abnormally segregated patterns of PCDH19 positive and negative cells in the developing mouse brain, which correlates with higher seizure susceptibility

PCDH19 is located on the X-chromosome that undergoes random X-chromosome inactivation in females,[8,20] it allows mosaic expression of PCDH19 positive and negative cells. It is hypothesized that abnormal interaction between these two populations of cells in the brain is the underlying mechanism of causing EFMR and this cellular mechanism is known as 'cellular interference'.[19] To study the functional consequences of the mosaic expression of PCDH19 in the mice brain, B6;129-Hprt$^{tm2(CMV\text{-}tdTomato)Nat}$/J mice (tdTomato (tdT) reporter gene targeted at Hprt locus on X-chromosome)[45] were crossed with *Pcdh19* KO mice. Firstly, CMV-Cre mice were crossed with HPRT$^{LSL\text{-}tdT}$ mice to remove LoxP-stop-LoxP (LSL) to generate CMV-Cre; HPRT$^{LSL\text{-}tdT}$ mice, so tdT is activated in all cells (Figure 1, upper left). For *Pcdh19* KO mice, the exon 1, 2 and 3 was replaced with β-gal/neoR fusion cassette to create *Pcdh19* KO mice (Figure 1, upper right).[21] Next, CMV-Cre; HPRT$^{LSL\text{-}tdT}$ female mice were crossed with *Pcdh19* KO male mice, and unexpected random X-chromosome recombination between *Pcdh19* gene (133.6 Mb) and *tdT* (53 Mb) occurred and created two different recombinant male mice; X'$_{tdT}$Y(KO-tdT) and X$_{tdT}$Y(WT-tdT) (Figure 1, below). The distance between two genes are calculated to be 80.6Mb and since it was reported that the genome-wide average recombination rates of mouse X-chromosome are 0.4 cM/Mb,[46] this random recombination rate of *Pcdh19* and *tdT* are calculated to be about 30% (80.6 Mb x 0.4

cM/Mb). For KO-tdT male mice, the tdT expressing cells are predicted to be activated and have *Pcdh19* null genes in the same X-chromosome. For WT-tdT male mice, *Pcdh19* gene is located with *tdT* in the same X-chromosome instead of the null gene. Next, KO-tdT male recombinant mouse was crossed once with HET (XX') female to obtain F1 $X'_{tdT}X$ (HET-tdT) and $X'_{tdT}X'$ (KO-tdT) female littermates and WT-tdT male recombinant mouse was crossed with XX (WT) female to generate F1 WT-tdT) female mice (Figure 13A). Only littermates from F1 generation were used in this experiment in order to preserve this random X-recombination and prevent another X-recombination from happening. Using these recombinant female mice, I was able to observe cellular distribution patterns depending on the PCDH19 expression. The brain sections of HET-tdT female mice at E14.5 (b, e of Figure 13B) showed abnormal sorting patterns, which were recently reported in another mice model.[16] However, this unique pattern was absent in both WT-tdT female (a, d of Figure 13B) and KO-tdT female (c, f of Figure 13B) recombinant mice, having uniform cell population of either PCDH19-positive or -negative cells. Although, two independent PCDH19 KO mice models from two distinctive research group fail to display naturally induced seizure phenotypes, which is one of the major symptoms seen in EFMR patients,[21,22] pharmacologically induced seizures were reported in P7 pups when PCDH19 was downregulated.[47] This encouraged me to evaluate pharmacologically induced seizure susceptibility levels of *Pcdh19* KO mice including all genotypes using most commonly used seizure induced drug in rodent, pilocarpine. Notably, the latency to the first generalized seizure were significantly lower in XX' mice compared to both XX and X'X', which indicates that XX' mice have lower seizure susceptibility (Figure 14A-B). There were no significant differences in the seizure latency with male mice (Figure 14C-D). The female HET-

tdT mouse have abnormal segregation of the PCDH19- positive and –negative cells in the developing brain, as shown by the patterns, and they were also more susceptible to pilocarpine-induced seizures. The mosaic expression of *Pcdh19* in HET-tdT female mice generate the abnormal segregation of cells in the developing cortex, correlating with higher seizure susceptibility. Since the epileptic symptoms of EFMR only appear in heterozygote female patient with mosaic expression of *PCDH19*, the aberrant cell sorting of WT and null PCDH19 cells can occur during human cortical development, altering the normal brain network.

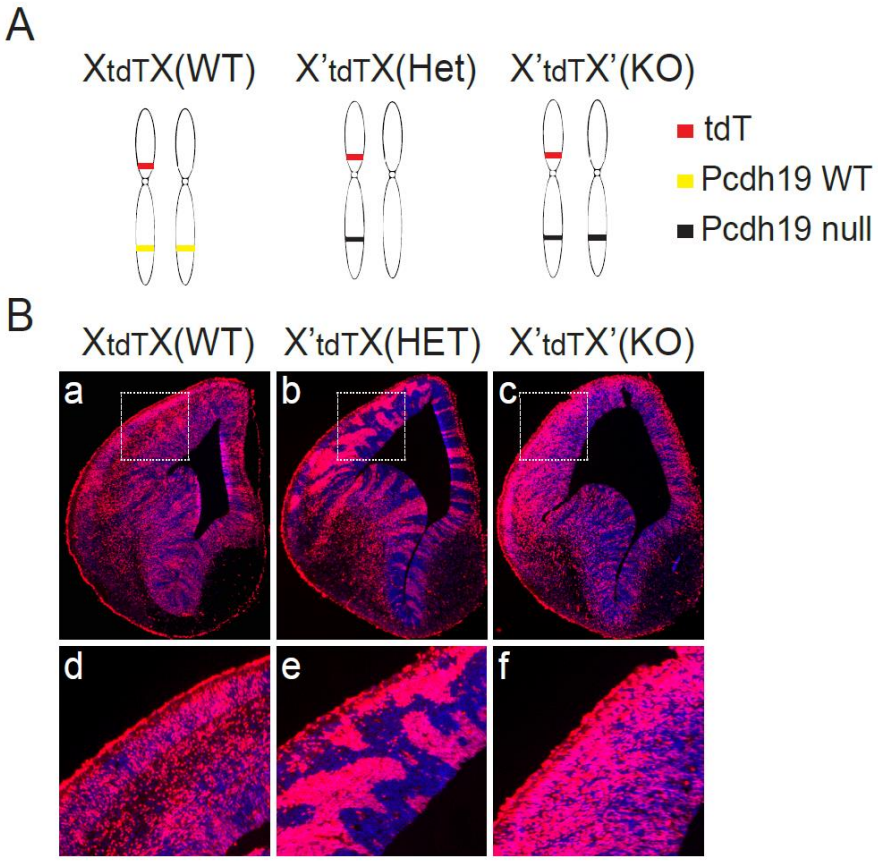

Figure 13. Unique segregation of PCDH19 expression pattern shown in the developing brain of the recombinant female (X'$_{tdT}$X) mice. A. Diagrams representing a random recombination between tdT and *Pcdh19* WT or null genes in the same X-chromosome. B. tdT expression patterns of recombinant female mice brains at E14.5. For X$_{tdT}$X (WT-tdT) female mice (a, d), tdT expressing cells represent activated PCDH19 positive cells, but for both HET-tdT (b, e) and X'$_{tdT}$X' (KO) (c, f) mice, tdT expressing cells represent activated PCDH19 negative cells.

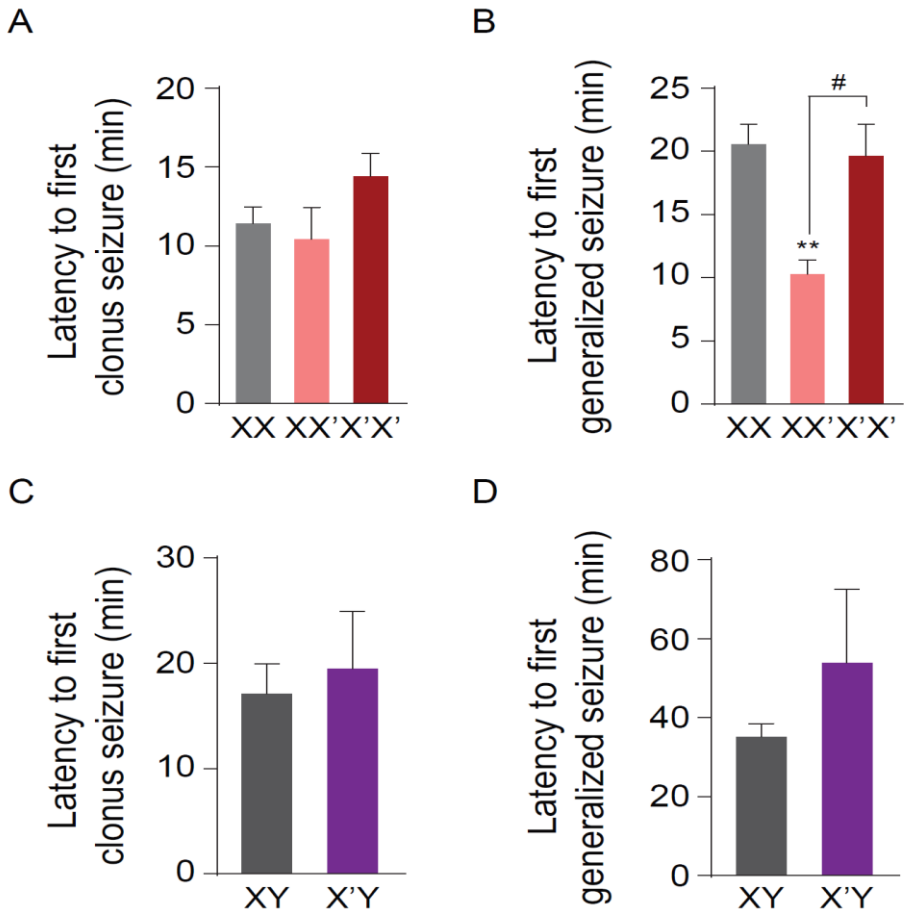

Figure 14. Increased seizure susceptibility in female HET (XX') mice with mosaic expression of PCDH19. A. Quantification of time latency to induce the first clonus seizure of different genotypes (XX, WT; XX', HET; X'X', KO) in female *Pcdh19* KO mice. B. Quantification of time latency to induce the first generalized seizure of different genotypes in female *Pcdh19* mutant mice. XX' showed shorter latency to reach generalized seizure than both XX and X'X' mice. C. Quantification of time latency to induce the first clonus seizure of different genotypes (XY, WT; X'Y, KO) in male *Pcdh19* mutant mice. D. Quantification of time latency to induce the first generalized seizure of different genotypes in male *Pcdh19* mutant mice. For

female mice, XX (n= 13), XX’ (n= 14), X’X’ (n= 16) and for male mice (n= 5 per group) were used. One-way ANOVA, followed by Bonferroni *post-hoc* test, $^{**}p < 0.01$ compared with XX, $\#p < 0.05$. All data are presented as means ± s.e.m

IV. DISCUSSION

This study illustrated the molecular characteristics of PCDH19 and several *PCDH19* mutations that are closely related to cause EFMR. Up until now, 271 cases of different disease-causing *PCDH19* mutations have been found, about 40% nonsense and frameshift mutations in *PCDH19* where premature termination codon had been placed, and 60% missense mutations, where a single amino acid sequence had been mutated.[48-50] Despite the fact that many mutations have been reported, no one yet fully understands how these mutations lead to EFMR. It is generally shared that nonsense mutation would give rise to cells expressing no PCDH19 protein. Through random X-inactivation in heterozygous mutant females, it gives rise to mosaic expression of PCDH19-positive and -negative cells (seen in clinical phenotype) which is considered as the main process of causing EFMR. Still, there are no experimental evidence to support how this loss of function by nonsense mutations in *PCDH19* could lead to EFMR at tissue levels. Thus, the consequence of a missense mutations is also difficult to predict.[8,51] The missense mutations of *PCDH19* are commonly believed to be loss of function mutations, acting similar to nonsense mutations. Some groups had already suggested that the missense mutations would adversely affect the calcium-binding sites near the EC domains, impairing the adhesive function of PCDH19.[11] In the part 1 of my thesis, I have experimentally demonstrated that at least some of the missense mutations like V441E and N557K rather increased surface protein levels. The increased surface expression levels of missense-mutated PCDH19 proteins are resistant to secretase activities, and accumulated at the cell surface. This abnormally elevated surface protein levels of these PCDH19 mutants seem to result in a gain of function of the proteins in the cell

aggregation assay. It is already well known that classical cadherins, such as N- and E-cadherin, undergo proteolytic cleavage.[52,53] Not surprisingly, cleavage of PCDH19 is also subjected to similar proteolytic process. However, this is the first report showing that human disease-causing mutations in a cadherin superfamily molecules inhibit its cleavage by α-secretase. Normally PCDH19 translocates to the nucleus during neuronal development in primary cultured neurons (Figure 6D), while missense-mutated PCDH19 remains in the cytosol. Combined with the fact that missense-mutated PCDH19 are resistant to the α-secretase dependent cleavage process, it leaves 'uncut' proteins on the cell surface (Figure 6C, 7), elevating the surface protein levels that otherwise decline as the brains mature (Figure 4B-C). The normal expression level of PCDH19 gradually increases during cortical developmental period up until P7 in mice, assuming that WT is also resistant to proteolytic cleavage for unknown mechanism until this period. After P7, the decline of PCDH19 protein expressions might be regulated through proteolytic cleavage, therefore decreasing the expressions on the cell surface. Assuming this decline of PCDH19 protein level after P7 is a normal physiological process, this time point might be a critical period for missense-mutated PCDH19 to have the pathogenic effects. In *PCDH19* heterozygous females, there are two different populations of cells and each cell expresses either WT or PCDH19-missense mutants. Therefore, cells with PCDH19-missense mutations would still be fully expressed on the cell surface while cells expressing WT would normally undergo cleavage processes. This could induce the imbalance of PCDH19 expressions after P7. Nonetheless, this is not the case for PCDH19 nonsense mutations because they do not produce PCDH19 proteins from much earlier time point in development. Considering the 'cellular interference' as the mechanism for inducing EFMR, PCDH19-missense mutations give us an

insight that imbalanced PCDH19 expression levels among cells can also cause problems in the brain development. This imbalanced expression of PCDH19 can be induced by co-existence of normal and null *PCDH19*-nonsense allele (no PCDH19 expression) as well as of normal and *PCDH19*-missense allele (higher expression of PCDH19). Unlike the popular belief that missense mutations would also be loss of function mutations (similar to the nonsense mutations), the action mechanism of missense mutations could be different from nonsense mutations in causing EFMR. Cellular interference induces abnormal cell-cell interaction in the mosaicism, which is thought to be an important underlying mechanism of both craniofrontonasal syndrome and EFMR.[19,54] Therefore, this uneven PCDH19 expression of cells would abnormally interfere with each other and this can lead to some defects in developmental process such as synapse formation, neuronal proliferation, and migration. This theory and its functional consequences were further investigated in the *in vitro* cell aggregation assay. Some mutations that are resistant to secretase activities, therefore having higher surface expression (i.e. group 1 mutations), have cell aggregation abilities similar to WT in the homogeneous condition (mixture of identical populations of the cells). When PCDH19-mutant expressing cells were mixed with WT expressing cells (to mimic mosaic conditions), it seemed to increase its adhesive affinities and form abnormal size of cell aggregates. However, this phenotype was not replicated in other missense mutations (group 2 mutations). This shows that the missense mutations could be divided into two different groups; some are gain-of-function mutations and others are loss-of-function mutations acting similarly to the nonsense mutations. In contrary to the earlier hypothesis that cells with *PCDH19*-missense mutations may impair the normal PCDH19-mediated cell-to-cell adhesion activities, my data showed that some of the missense mutations rather

increased its adhesive affinities dramatically when mixed with WT cells.

Two different *Pcdh19* KO mouse models were reported by two independent groups.[21,22] However, both groups of *Pcdh19* KO mice models displayed neither obvious defects in the gross structure of the brain nor any anxiety and seizure-related behavioural impairments. Since they did not manifest clinical phenotypes of EFMR, these *Pcdh19* KO models were not believed to be eligible to study clinical features of EFMR. However, recently Pederick et al. revealed the relevant EFMR phenotypes in the *Pcdh19* KO models. This group showed abnormal segregation of the PCDH19-positive and –negative cells in the *HA-FLAG*/β-*Geo* knock-in heterozygous (HET) female KO mice brain during the cortical development. Moreover, these HET KO female mice also showed the altered brain activity of electrocorticogram (ECoG) analysis.[16] These results have demonstrated the typical clinical phenotypes of EFMR

When this brain phenotype was reported, I was also analyzing the mice brain patterns for the part 2 of my thesis (Figure 13B) using a tdT-recombinant mouse model. This recombinant mice were generated by random X-chromosomal recombination between *Pcdh19* and *tdT* genes during mating of *Pcdh19* KO and *CMV-Cre;Hprt-LSL-tdT* mice to label PCDH19 -positive or -negative cells with tdT. This unique brain patterns are only observed in the *Pcdh19* HET KO female mice because they have the mosaic expression of PCDH19 protein. Two different population of PCDH19 -positive and –negative expressing cells would have different cell-to-cell adhesion affinities, therefore causing cells to abnormally segregate in the developing brain. This phenotype was absent in both WT and *Pcdh19* KO female mice (with uniform expression of WT or *Pcdh19* null cells). My study also demonstrated that *Pcdh19* HET KO female mice were more susceptible to pilocarpine-induced seizures compared to WT and *Pcdh19* homozygous KO female

mice. This emphasizes the 'cellular interference' theory by experimentally showing the abnormal interactions between PCDH19-positive and –negative cells during cortical development, causing seizure-like behaviours seen in EFMR. The fact that *Pcdh19* HET KO female mice with 'patterned brain' displayed seizure related phenotypes in both my study and EcoG analysis,[16] I showed the strong correlation of cell sorting and seizure phenotypes in relation to the unique genotype-phenotype relation of EFMR. During cortical development, this abnormal sorting patterns have potential to disturb the normal distribution of neurons or functionally perturb the normal neuronal connections and consequently cause seizure-like brain activities. The development timing of neurons is crucial in establishing the normal connection and network. Therefore, improper timing of neuronal development would cause neurons to abnormally interact with one another that can eventually lead to dysfunction of brain network, like epilepsy. The inhibition and excitation imbalance at the synaptic level play a crucial role in causing seizure. Since the role of PCDH19 in GABAergic transmission have been recently suggested,[47] I additionally wanted to investigate the neuronal properties of sorted cells in *Pcdh19* HET KO female mice brain related to the excitatory-inhibitory ratio. The imbalance of the ratio between glutamatergic-GABAergic neurons have not only been considered to be the important mechanism for seizure, but also in other neuropsychiatric diseases like autism.[55,56] In order to investigate whether the seizure phenotypes seen in *Pcdh19* HET KO female mice are due to any disruption of the glutamatergic-GABAergic ratio, immunohistochemistry of parvalbumin-expressing (PV) inhibitory neurons were performed. Interestingly, *Pcdh19* HET KO female mice exhibited significant decrease in the number of PV-inhibitory neurons compared to both WT and *Pcdh19* homozygous KO mice (Figure 15A-B). This decrease in the number of PV-inhibitory

neurons is responsible for the excitatory-inhibitory imbalance, and it leads to the disruption of neuronal network. This disturbance of the excitatory-inhibitory balance in the brain would lead to seizure seen in EFMR-affected females. Since PV-inhibitory neurons were only disturbed in *Pcdh19* HET KO female mice, the mosaic expression of PCDH19 somehow led to the disruptions of PV-neuron network activity that manipulates the excitatory-inhibitory balance of the brain, but further research is necessary to establish this.

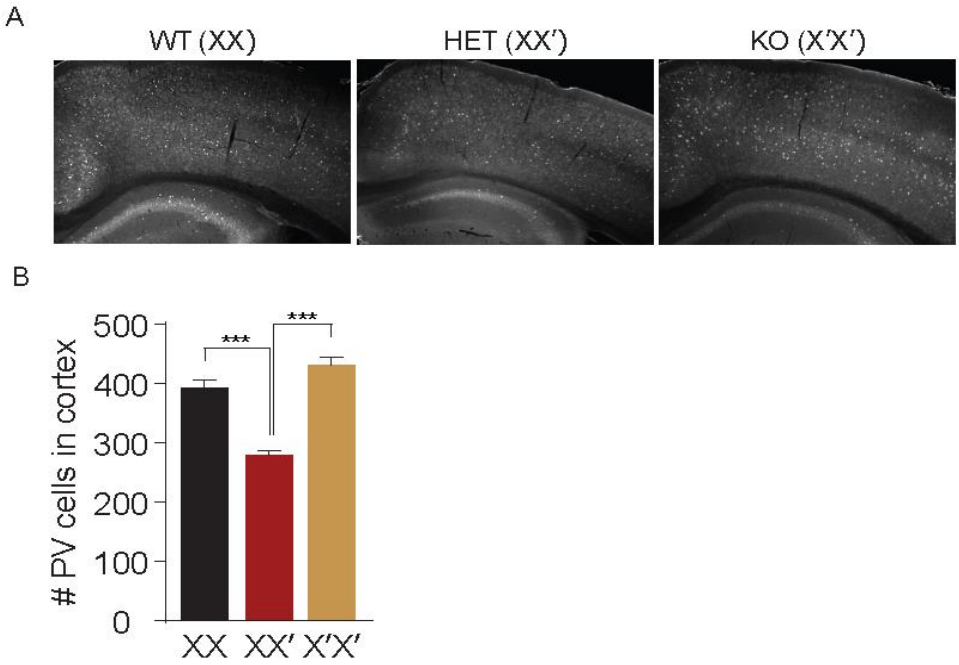

Figure 15. Decreased number of PV-inhibitory neurons in female HET(XX') mice. A. Representative photomicrographs of cortex showing PV immunohistochemistry in coronal sections of *Pcdh19* mutant female mice of all three genotypes (form the left, WT (XX), HET (XX') and KO (X'X')) at 8 weeks old. B. Quantification analysis of PV-cells in the cortex. One-way ANOVA, followed by Bonferroni *post-hoc* test, ***$p < 0.001$. All data are presented as means ± s.e.m

EFMR is a disorder with unusual X-linked mode of inheritance where symptoms only appear in females with heterozygous *PCDH19* mutation, not in hemizygous mutant males with no PCDH19. However, there is no reported case of females with homozygous *PCHD19* mutations, hence it is hard to know the effects of complete absence of PCDH19 in females. The fact that hemizygous mutant males with no PCDH19 didn't show any EFMR symptoms therefore, I can only speculate asymptomatic phenotypes of females with complete absence of PCDH19. Here in part 2, I have shown that *Pcdh19* homozygous KO females have even distribution of the PCDH19 null cells and this complete absence of the PCDH19 does not induce a seizure-like symptom in pilocarpine-induced rodent seizure models. The fact that the high seizure susceptibility was only observed in *Pcdh19* HET KO female mice, not in WT and *Pcdh19* hemizygous KO male and homozygous KO female mice, suggests the importance of homogeneous distribution of PCDH19 in the brain for the normal brain activity. In this study, I was only able to study the consequences of having two populations of PCDH19 –positive and –negative cells using *Pcdh19* KO mice. If *Pcdh19* (V441E)-missense mutant mice model is available in the future, it would be very interesting to study the brain patterns of HET KO female mice to see if two different population of cells (WT and V441E mutant) would atypically aggregate in unusual patterns during early cortical development. This patterns would be quite distinct from the segregated patterns of *Pcdh19* KO mice. Further investigation is necessary to establish the exact mechanism of how missense mutations cause EFMR, but this study provides with some potential possibility that they are gain of function mutations that also disturb the normal neuronal network of the brain.

V. CONCLUSION

In Part 1, I showed that PCDH19 plays critical roles in the early brain development, because the expression levels peak around the first postnatal week (P7) and rapidly decline after this period in the mice brain. Also, the PCDH19 on the cell surface undergoes secretase-dependent cleavage pathway and identified that some of the missense mutations of PCDH19 are resistant to this cleavage processes. As a consequence, theses missense mutations rather increases surface expression levels. I have also characterized the adhesive features of PCDH19 and PCDH19 mutants using cell aggregation assay and found that some group of missense mutations are gain of function mutations because they promote the formation of cell aggregates in the mosaic environment. I proposed a new schematic model to explain the PCDH19 adhesion properties. Through this schematic model, I demonstrated the abnormal adhesive functions of some of the PCDH19-missense mutations (V441E and N557K) in the environment where WT cells were mixed.

In part 2, using *Pcdh19* KO mouse model, I demonstrated the segregated patterns of PCDH19-positive and -negative cells in the developing brain of the *Pcdh19* HET KO female mice. This abnormal sorting pattern of the *Pcdh19* HET KO female brain phenotypically correlate with higher seizure susceptibility than WT and *Pcdh19* KO mice, both having no apparent brain patterns. Furthermore, the deficit of PV-inhibitory neuron was only noticeable in *Pcdh19* HET KO female mouse brain. This data indicates that the mosaic expression of PCDH19 disrupts the normal cell-cell interaction and it leads to deficit in PV-inhibitory neurons that likely to alter cortical network activities inducing seizures.

Overall, this work contributes to our understanding of the role of PCDH19 in brain

development and the functional consequences of having EFMR-causing mutations. The fact that *PCDH19* missense mutations could cause imbalanced expression of PCDH19, bring us a step closer to understand the complex mechanism of EFMR. I hope this would contribute to provide an insight into the understanding of other genetic disorders with unusual genetic inheritance patterns.

REFERENCES

1. Steinberg MS. Differential adhesion in morphogenesis: a modern view. Curr Opin Genet Dev 2007;17:281-6.
2. Takeichi M. The cadherins: cell-cell adhesion molecules controlling animal morphogenesis. Development 1988;102:639-55.
3. Yagi T, Takeichi M. Cadherin superfamily genes: functions, genomic organization, and neurologic diversity. Genes Dev 2000;14:1169-80.
4. Hulpiau P, van Roy F. Molecular evolution of the cadherin superfamily. Int J Biochem Cell Biol 2009;41:349-69.
5. Takeichi M. Cadherin cell adhesion receptors as a morphogenetic regulator. Science 1991;251:1451-5.
6. Emond MR, Biswas S, Jontes JD. Protocadherin-19 is essential for early steps in brain morphogenesis. Dev Biol 2009;334:72-83.
7. Morishita H, Yagi T. Protocadherin family: diversity, structure, and function. Curr Opin Cell Biol 2007;19:584-92.
8. Dibbens LM, Tarpey PS, Hynes K, Bayly MA, Scheffer IE, Smith R, et al. X-linked protocadherin 19 mutations cause female-limited epilepsy and cognitive impairment. Nat Genet 2008;40:776-81.
9. Ishizuka K, Kimura H, Wang C, Xing J, Kushima I, Arioka Y, et al. Investigation of Rare Single-Nucleotide PCDH15 Variants in Schizophrenia and Autism Spectrum Disorders. PLoS One 2016;11:e0153224.
10. Wolverton T, Lalande M. Identification and characterization of three members of a novel subclass of protocadherins. Genomics 2001;76:66-72.
11. Cooper SR, Jontes JD, Sotomayor M. Structural determinants of adhesion by

Protocadherin-19 and implications for its role in epilepsy. Elife 2016;5.

12. Takeichi M, Abe K. Synaptic contact dynamics controlled by cadherin and catenins. Trends Cell Biol 2005;15:216-21.

13. Tsai NP, Wilkerson JR, Guo W, Maksimova MA, DeMartino GN, Cowan CW, et al. Multiple autism-linked genes mediate synapse elimination via proteasomal degradation of a synaptic scaffold PSD-95. Cell 2012;151:1581-94.

14. Hoshina N, Tanimura A, Yamasaki M, Inoue T, Fukabori R, Kuroda T, et al. Protocadherin 17 regulates presynaptic assembly in topographic corticobasal Ganglia circuits. Neuron 2013;78:839-54.

15. Tai K, Kubota M, Shiono K, Tokutsu H, Suzuki ST. Adhesion properties and retinofugal expression of chicken protocadherin-19. Brain Res 2010;1344:13-24.

16. Pederick DT, Richards KL, Piltz SG, Kumar R, Mincheva-Tasheva S, Mandelstam SA, et al. Abnormal Cell Sorting Underlies the Unique X-Linked Inheritance of PCDH19 Epilepsy. Neuron 2018;97:59-66.e5.

17. Scheffer IE, Turner SJ, Dibbens LM, Bayly MA, Friend K, Hodgson B, et al. Epilepsy and mental retardation limited to females: an under-recognized disorder. Brain 2008;131:918-27.

18. Juberg RC, Hellman CD. A new familial form of convulsive disorder and mental retardation limited to females. J Pediatr 1971;79:726-32.

19. Depienne C, Bouteiller D, Keren B, Cheuret E, Poirier K, Trouillard O, et al. Sporadic infantile epileptic encephalopathy caused by mutations in PCDH19 resembles Dravet syndrome but mainly affects females. PLoS Genet 2009;5:e1000381.

20. Cotton AM, Price EM, Jones MJ, Balaton BP, Kobor MS, Brown CJ. Landscape of DNA methylation on the X chromosome reflects CpG density, functional chromatin state and X-chromosome inactivation. Hum Mol Genet 2015;24:1528-39.

21. Pederick DT, Homan CC, Jaehne EJ, Piltz SG, Haines BP, Baune BT, et al. Pcdh19 Loss-of-Function Increases Neuronal Migration In Vitro but is Dispensable for Brain Development in Mice. Sci Rep 2016;6:26765.

22. Hayashi S, Inoue Y, Hattori S, Kaneko M, Shioi G, Miyakawa T, et al. Loss of X-linked Protocadherin-19 differentially affects the behavior of heterozygous female and hemizygous male mice. Sci Rep 2017;7:5801.

23. Bankstahl M, Muller CJ, Wilk E, Schughart K, Loscher W. Generation and characterization of pilocarpine-sensitive C57BL/6 mice as a model of temporal lobe epilepsy. Behav Brain Res 2012;230:182-91.

24. Cavalheiro EA, Santos NF, Priel MR. The pilocarpine model of epilepsy in mice. Epilepsia 1996;37:1015-9.

25. Takeichi M, Nakagawa S. Cadherin-dependent cell-cell adhesion. Curr Protoc Cell Biol 2001;Chapter 9:Unit 9.3.

26. Xu SY, Wu YM, Ji Z, Gao XY, Pan SY. A modified technique for culturing primary fetal rat cortical neurons. J Biomed Biotechnol 2012;2012:803930.

27. Gaitan Y, Bouchard M. Expression of the delta-protocadherin gene Pcdh19 in the developing mouse embryo. Gene Expr Patterns 2006;6:893-9.

28. Kim SY, Chung HS, Sun W, Kim H. Spatiotemporal expression pattern of non-clustered protocadherin family members in the developing rat brain. Neuroscience 2007;147:996-1021.

29. Kolc KL, Sadleir LG, Scheffer IE, Ivancevic A, Roberts R, Pham DH, et al.

A systematic review and meta-analysis of 271 PCDH19-variant individuals identifies psychiatric comorbidities, and association of seizure onset and disease severity. Mol Psychiatry 2018; doi:10.1038/s41380-018-0066-9.

30. Hayashi S, Takeichi M. Emerging roles of protocadherins: from self-avoidance to enhancement of motility. J Cell Sci 2015;128:1455-64.

31. Marambaud P, Shioi J, Serban G, Georgakopoulos A, Sarner S, Nagy V, et al. A presenilin-1/gamma-secretase cleavage releases the E-cadherin intracellular domain and regulates disassembly of adherens junctions. Embo j 2002;21:1948-56.

32. Reiss K, Maretzky T, Ludwig A, Tousseyn T, de Strooper B, Hartmann D, et al. ADAM10 cleavage of N-cadherin and regulation of cell-cell adhesion and beta-catenin nuclear signalling. Embo j 2005;24:742-52.

33. Maretzky T, Reiss K, Ludwig A, Buchholz J, Scholz F, Proksch E, et al. ADAM10 mediates E-cadherin shedding and regulates epithelial cell-cell adhesion, migration, and beta-catenin translocation. Proc Natl Acad Sci U S A 2005;102:9182-7.

34. Brown MS, Ye J, Rawson RB, Goldstein JL. Regulated intramembrane proteolysis: a control mechanism conserved from bacteria to humans. Cell 2000;100:391-8.

35. Edwards DR, Handsley MM, Pennington CJ. The ADAM metalloproteinases. Mol Aspects Med 2008;29:258-89.

36. Reiss K, Saftig P. The "a disintegrin and metalloprotease" (ADAM) family of sheddases: physiological and cellular functions. Semin Cell Dev Biol 2009;20:126-37.

37. Kiecker C, Lumsden A. Compartments and their boundaries in vertebrate

brain development. Nat Rev Neurosci 2005;6:553-64.

38. Zipursky SL, Sanes JR. Chemoaffinity revisited: dscams, protocadherins, and neural circuit assembly. Cell 2010;143:343-53.

39. Yoshida C, Takeichi M. Teratocarcinoma cell adhesion: identification of a cell-surface protein involved in calcium-dependent cell aggregation. Cell 1982;28:217-24.

40. Hatta K, Nose A, Nagafuchi A, Takeichi M. Cloning and expression of cDNA encoding a neural calcium-dependent cell adhesion molecule: its identity in the cadherin gene family. J Cell Biol 1988;106:873-81.

41. Hirano S, Takeichi M. Cadherins in brain morphogenesis and wiring. Physiol Rev 2012;92:597-634.

42. Hayashi S, Inoue Y, Kiyonari H, Abe T, Misaki K, Moriguchi H, et al. Protocadherin-17 mediates collective axon extension by recruiting actin regulator complexes to interaxonal contacts. Dev Cell 2014;30:673-87.

43. Hirano S, Yan Q, Suzuki ST. Expression of a novel protocadherin, OL-protocadherin, in a subset of functional systems of the developing mouse brain. J Neurosci 1999;19:995-1005.

44. Rubinstein R, Thu CA, Goodman KM, Wolcott HN, Bahna F, Mannepalli S, et al. Molecular logic of neuronal self-recognition through protocadherin domain interactions. Cell 2015;163:629-42.

45. Wu H, Luo J, Yu H, Rattner A, Mo A, Wang Y, et al. Cellular resolution maps of X chromosome inactivation: implications for neural development, function, and disease. Neuron 2014;81:103-19.

46. Jensen-Seaman MI, Furey TS, Payseur BA, Lu Y, Roskin KM, Chen CF, et al. Comparative recombination rates in the rat, mouse, and human genomes.

Genome Res 2004;14:528-38.

47. Bassani S, Cwetsch AW, Gerosa L, Serratto GM, Folci A, Hall IF, et al. The female epilepsy protein PCDH19 is a new GABAAR-binding partner that regulates GABAergic transmission as well as migration and morphological maturation of hippocampal neurons. Hum Mol Genet 2018;27:1027-38.

48. Depienne C, LeGuern E. PCDH19-related infantile epileptic encephalopathy: an unusual X-linked inheritance disorder. Hum Mutat 2012;33:627-34.

49. Kolc KL, Sadleir LG, Scheffer IE, Ivancevic A, Roberts R, Pham DH, et al. A systematic review and meta-analysis of 271 PCDH19-variant individuals identifies psychiatric comorbidities, and association of seizure onset and disease severity. Mol Psychiatry 2019;24:241-51.

50. Niazi R, Fanning EA, Depienne C, Sarmady M, Abou Tayoun AN. A mutation update for the PCDH19 gene causing early-onset epilepsy in females with an unusual expression pattern. Hum Mutat 2019;40:243-57.

51. Homan CC, Pederson S, To TH, Tan C, Piltz S, Corbett MA, et al. PCDH19 regulation of neural progenitor cell differentiation suggests asynchrony of neurogenesis as a mechanism contributing to PCDH19 Girls Clustering Epilepsy. Neurobiol Dis 2018;116:106-19.

52. Junghans D, Haas IG, Kemler R. Mammalian cadherins and protocadherins: about cell death, synapses and processing. Curr Opin Cell Biol 2005;17:446-52.

53. Posthaus H, Dubois CM, Laprise MH, Grondin F, Suter MM, Muller E. Proprotein cleavage of E-cadherin by furin in baculovirus over-expression system: potential role of other convertases in mammalian cells. FEBS Lett 1998;438:306-10.

54. Twigg SR, Babbs C, van den Elzen ME, Goriely A, Taylor S, McGowan SJ, et al. Cellular interference in craniofrontonasal syndrome: males mosaic for mutations in the X-linked EFNB1 gene are more severely affected than true hemizygotes. Hum Mol Genet 2013;22:1654-62.

55. Antoine MW, Langberg T, Schnepel P, Feldman DE. Increased Excitation-Inhibition Ratio Stabilizes Synapse and Circuit Excitability in Four Autism Mouse Models. Neuron 2019;101:648-61.e4.

56. Fan X, Gaspard N, Legros B, Lucchetti F, Ercek R, Nonclercq A. Automated epileptic seizure detection based on break of excitation/inhibition balance. Comput Biol Med 2019;107:30-8.

ABSTRACT (in Korean)

지적 장애를 동반한 여성 제한적 간질(EFMR)을 유발하는 *PCDH19* 유전자 변이의 분자기능학적 기전 규명

<지도교수 김 철 훈>

연세대학교 대학원 의과학과

임 지 수

지적 장애를 동반한 여성 제한적 뇌전증 (Epilepsy in females with mental retardation, EFMR)은 X-염색체에 위치한 *PCDH19* (Protocadherin-19)유전자 변이에 의해 발병한다. EFMR은 비정상적인 X-연관 유전을 따르는 질환으로 남성의 경우 증상이 나타나지 않고, 이형접합체 (heterozygous)여성에서만 특이적으로 나타난다. 이형접합체 여성에서는 무작위 X-염색체 불 활성화의 영향으로 정상세포와 PCDH19 돌연변이 세포들이 섞여 있는 모자이크 현상이 나타나는데, 세포 간섭 (cellular interference)에 의해 정상적인 뇌세포 상호작용을 변화시켜 해롭게 함으로 EFMR을 발병한다는 것이다. 현재까지 EFMR 환자에서 보고된 *PCDH19* 돌연변이들 중 절반이 미스센스 돌연변이, 나머지 절반은 넌센스 돌연변이로 알려져 있다. *PCDH19*의 미스센스 돌연변이가 생기면 PCDH19를 전혀 발현 하지 않는 넌센스 돌연변이처럼 기능을 상실할 것이라고 추측되고 있지만, 아직까지 미스센스 돌연변이의 분자생화학적 기능이상이나 EFMR 발병 기전의 연관성에 대해서는 명확하게 연구 된 바

없다. 그러므로 본 연구 1부에서는 세포막에 정상 PCDH19 발현이 초기 뇌 발달과정에 증가했다가 P7 이후로 감소하는 것을 확인함으로써 초기 발달에 중요한 역할을 한 다는 것을 밝혔고, 발달과정에서 세크래타제(secretase)에 의해 잘린 다는 것을 확인하였다. 하지만 미스센스 돌연변이가 생기면 세크래타제에 저항성이 생겨 잘리지 않고 세포막에 남아 발현양이 증가하는 것을 보았고, 이런 현상이 이들의 접착 기능에 미치는 영향을 보기 위해 세포 응집 검사 (cell aggregation assay)를 진행하였다. 그 결과 두 가지 다른 세포를 섞어준 인공 모자이크 환경에서 몇몇 돌연변이가 비정상적 세포 응집을 촉진하는 것을 확인함으로써 미스센스 돌연변이가 오히려 기능획득변이라는 것을 밝혔다. 2부에서는 야생형 (wild-type) 암컷 마우스 및 *Pcdh19*가 양쪽 X-염색체에서 결여된 동형접합체 (homozygous KO) 암컷 마우스와 달리 한쪽에서만 결여된 이형접합체 암컷 마우스에서만 PCDH19을 발현하는 세포와 그렇지 않은 세포들이 분리되는 '패턴'을 보여주었다. 이런 패턴을 보이는 이형접합체 암컷 마우스에서만 필로카르핀 (pilocarpine)으로 유발된 발작에 대하여 높은 감수성을 보였으며, 이를 통해 비정상적으로 세포가 분류되는 패턴이 정상 뇌 발달을 방해하여 발작을 유발하는 것과의 연관성을 증명하였다. 결론적으로 EFMR은 정상세포가 PCDH19을 발현하지 않는 넌센스 돌연변이나 높은 PCDH19 발현양을 보이는 미스센스 돌연변이와 함께 공존할 때, 어떠한 경우라도 불균형을 일으켜 비정상적인 세포 상호작용을 촉진하여 발병한다는 것을 시사한다. 이러한 특이적 유전병의 메커니즘을 이해하는 것은 아직 밝혀지지 않은 수많은 다른 희귀 질환을 이해하는데도 큰 도움이 될 것으로 기대된다.

핵심되는 말: 여성 제한적 뇌전증(EFMR), 지적장애, 프로토카데린19 (pcdh19), 모자이크 현상, 뇌전증, 불활성 X염색체, 세포 간섭

PUBLICATION LIST

1. **Lim J**, Kim E, Noh HJ, Kang S, Phillips BU, Kim DG, et al. Assessment of mGluR5 KO mice under conditions of low stress using a rodent touchscreen apparatus reveals impaired behavioural flexibility driven by perseverative responses. Mol Brain 2019;12:37.

2. Lee JH, **Lim J**, Chung YE, Chung SP, Park I, Kim CH, et al. Targeted Temperature Management at 33 degrees C or 36 degrees C Produces Equivalent Neuroprotective Effects in the Middle Cerebral Artery Occlusion Rat Model of Ischemic Stroke. Shock 2018;50:714-9.